Jet angular correlation in vector-boson fusion processes at hadron colliders

JHEP07(2009)101

(http://iopscience.iop.org/1126-6708/2009/07/101)

Published by IOP Publishing for SISSA

Received: *May 29, 2009*
Accepted: *July 13, 2009*
Published: *July 30, 2009*

Jet angular correlation in vector-boson fusion processes at hadron colliders

Kaoru Hagiwara,[a] **Qiang Li**[b] **and Kentarou Mawatari**[c,d]

[a] *KEK Theory Division and Sokendai, Tsukuba 305-0801, Japan*
[b] *Institut für Theoretische Physik, Universität Karlsruhe, Postfach 6980, D-76128 Karlsruhe, Germany*
[c] *Institut für Theoretische Physik, Universität Heidelberg, Philosophenweg 16, D-69120 Heidelberg, Germany*
[d] *School of Physics, Korea Institute for Advanced Study, Seoul 130-722, Korea*
E-mail: qliphy@particle.uni-karlsruhe.de, k.mawatari@thphys.uni-heidelberg.de

Abstract: Higgs boson and massive-graviton productions in association with two jets via vector-boson fusion (VBF) processes and their decays into a vector-boson pair at hadron colliders are studied. They include scalar and tensor boson production processes via weak-boson fusion in quark-quark collisions, gluon fusion in quark-quark (qq), quark-gluon (qg) and gluon-gluon (gg) collisions, as well as their decays into a pair of weak bosons or virtual gluons which subsequently decay into $\ell\bar{\ell}$, $q\bar{q}$ or gg. We give the helicity amplitudes explicitly for all the VBF subprocesses, and show that the VBF amplitudes dominate the exact matrix elements not only for the weak-boson fusion processes but also for all the gluon fusion processes when appropriate selection cuts are applied, such as a large rapidity separation between two jets and a slicing cut for the transverse momenta of the jets. We also show that our off-shell vector-boson current amplitudes reduce to the standard quark and gluon splitting amplitudes with appropriate gluon-polarization phases in the collinear limit. Nontrivial azimuthal angle correlations of the jets in the production and in the decay of massive spin-0 and -2 bosons are manifestly expressed as the quantum interference among different helicity states of the intermediate vector-bosons. Those correlations reflect the spin and the CP nature of the Higgs bosons and the massive gravitons.

Keywords: Beyond Standard Model, Higgs Physics, Hadronic Colliders

ArXiv ePrint: 0905.4314

doi:10.1088/1126-6708/2009/07/101

JHEP07(2009)101

Contents

JHEP07(2009)101

1 Introduction

Angular correlation of the two accompanying jets in Higgs boson productions at the CERN Large Hadron Collider (LHC) has been known as a potential tool to study its spin and CP nature, in the weak-boson fusion (WBF) $qq \to qqH$ processes [1], and in the gluon fusion (GF) plus dijet production processes [2–4], $qq \to qqH$, $qg \to qgH$ and $gg \to ggH$. In these reactions, the tensor structure of the Higgs coupling to weak bosons or gluons gives rise to the azimuthal angle correlation of the tagging jets; the WBF processes give flat $\Delta\phi_{jj}$ distribution, while the GF processes produce a distinct dip around $\Delta\phi_{jj} = \pi/2$. On the

other hand, in the case of a CP-odd Higgs boson, the azimuthal distribution is strongly enhanced around $\Delta\phi_{jj} = \pi/2$ in both the WBF and GF processes [1, 3, 4].[1]

So far, many studies on the azimuthal correlations in the Higgs + 2-jet events have been performed with higher-order QCD and electroweak corrections [8–13] including parton-shower effects [14, 15]. The present consensus seems to be that the azimuthal angle correlations predicted in the leading order may survive even after higher-order corrections are applied [13, 15]. It must be pointed out here that, due to the complicated matrix elements, it is not completely clear why the tensor structure of the couplings leads to such distinct azimuthal distributions, even though naive explanations have been presented [1, 2]. Since, in general, azimuthal angle dependence should be understood in terms of the quantum interference phases of the amplitudes with spin-full particles propagating along the polar axis, it may be valuable to reformulate the amplitudes for the Higgs production with two jets in such a way that their phases are shown explicitly.

As another interest to study the azimuthal angle correlation of the jets at the LHC, we attempt to apply it to other heavy particle productions. Here, we especially focus on massive-graviton productions in the localized gravity model of Randall and Sundrum (RS) [16], which has drawn a lot of attention in recent years because it brings a new solution to the hierarchy problem through an exponentially suppressed warp factor in a 5-dimensional non-factorizable geometry. Several phenomenological studies have been made on the Drell-Yan process for RS graviton resonances for its discovery and the determination of its spin-2 nature [17–23], including direct searches at the Tevatron [24], as well as the graviton + 1-jet productions [25]. Meanwhile massive-graviton productions in association with two jets may also have a great potential to scrutinize its properties as in the Higgs boson case. We note that the graviton + 2-jet productions in the large extra dimensions model [26] have recently been studied in ref. [27].

In this article, more generally, we study productions of a heavy color-singlet particle (X) in association with two jets via vector-boson fusion (VBF) processes at hadron colliders, $pp \to jjX$, which include WBF processes in quark-quark collisions and GF processes in quark-quark, quark-gluon and gluon-gluon collisions.[2] In particular, the reactions,

$$qq \to qqX, \quad qg \to qgX, \quad gg \to ggX, \tag{1.1}$$

are studied comprehensively as the leading-order subprocesses that lead to X + 2-jet events via VBF. In order to discern the phases of the amplitudes, we present the helicity amplitudes explicitly for all the VBF subprocesses at the tree level in terms of the specific kinematical variables, where the colliding vector-bosons have momenta back-to-back along the polar axis. Although the VBF amplitudes are valid only when the virtuality of the intermediate vector-bosons is smaller than their energies, as we will see later, they can dominate the exact matrix elements when appropriate selection cuts to the final states are applied, such as a large rapidity separation between two tagging jets and a slicing cut for the transverse momenta of the jets. We also show that our off-shell vector-boson current

[1] Azimuthal correlations in diffractive processes have also been discussed in refs. [5–7].

[2] Weak-boson fusion is sometimes referred to as VBF. In this paper, however, we refer to the fusion processes of all the standard model vector-bosons (W, Z, γ, g) as VBF, including WBF and GF processes.

JHEP07(2009)101

amplitudes reduce to the standard quark and gluon splitting amplitudes with appropriate phases in the collinear limit.

As for the produced heavy particles, we study neutral CP-even and CP-odd Higgs bosons and RS massive gravitons, and show that nontrivial azimuthal angle correlations of the jets in the production of massive spin-0 and -2 bosons are manifestly expressed as the quantum interference among different helicity states of the intermediate vector-bosons. Those correlation reflects the spin and the CP nature of the Higgs bosons and the massive gravitons. We do not consider massive spin-1 particles because the Landau-Yang theorem forbids production of a color-singlet spin-1 particle in fusions of two on-shell photons or gluons [28], and our approximation fails when their virtuality is large enough to give significant amplitudes.

Besides jet angular correlations in the production processes, the decay distributions and correlations of heavy particles are also promising tools to determine their properties, and extensive studies have been made especially for the Higgs bosons, e.g. $H \to ZZ \to (\ell\bar{\ell})(\ell\bar{\ell})$ [29–33]; see also review papers [34, 35] and references therein. The above decay process is related by crossing symmetry to the WBF Higgs production process, $qq \to qqH$, and hence it may be useful to compare the production correlations with the decay correlations. Therefore, we also consider X decays into a pair of weak-bosons or gluons which subsequently decay into $\ell\bar{\ell}$, $q\bar{q}$ or gg, and present the helicity amplitudes and the azimuthal angle correlations of the jets (and/or leptons), by comparing with those in the production processes.

The article is organized as follows. In section 2, we introduce the formalism of the helicity amplitudes and the density matrices for the X production with two jets via VBF and the X decay into a vector-boson pair. In section 3 we define kinematical variables relevant to our analysis for the production and decay processes. In section 4, we present all the helicity amplitudes explicitly for the off-shell vector-boson currents and the off-shell VBF processes. We also discuss the relation between our current amplitudes and the standard parton splitting amplitudes. In section 5, we demonstrate that the VBF amplitudes dominate the exact matrix elements when appropriate selection cuts to the final states are applied, and then discuss azimuthal angle correlations of the jets in the Higgs boson and massive-graviton productions. We also consider the decay correlations of the heavy particles. Finally section 6 summarizes our findings.

We include three appendices. Appendix A gives the wavefunction and the vertices for a spin-2 particle. In appendix B we show the relation between wavefunctions and Wigner's d functions. Appendix C presents the angular distributions for the massive-graviton decays, $G \to VV \to (f\bar{f})(f\bar{f})$.

2 Helicity formalism

In this section, we give the helicity amplitude formulae and the density matrix formalism for heavy particle (X) productions in association with two jets via VBF processes, and also those for its decay into a (virtual) vector-boson pair which subsequently decay into $\ell\bar{\ell}$, $q\bar{q}$ or gg.

JHEP07(2009)101

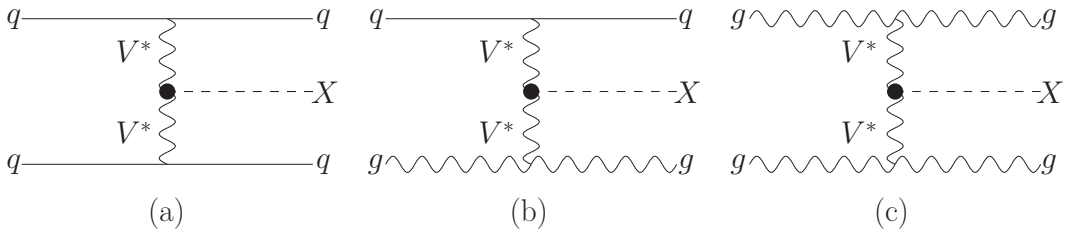

Figure 1. Feynman diagrams for the VBF subprocesses: (a) $qq \to qqX$, (b) $qg \to qgX$, and (c) $gg \to ggX$.

X + 2-jet productions via VBF at hadron colliders, $pp \to jjX$, can proceed through the subprocesses:

$$qq \to qqV^*V^* \to qqX \qquad (V = W,\, Z,\, \gamma,\, g), \tag{2.1a}$$

$$qg \to qgV^*V^* \to qgX \qquad (V = g), \tag{2.1b}$$

$$gg \to ggV^*V^* \to ggX \qquad (V = g), \tag{2.1c}$$

where V^* is a t-channel intermediate vector-boson and q stands for a quark or antiquark of any flavors. A representative Feynman diagram for each subprocess is shown in figure 1(a), (b), and (c), respectively, for the subprocess (2.1a), (2.1b), and (2.1c). Each subprocess receives contributions not only from the above VBF diagram but also from all the other diagrams of the same order, in order to make the gauge-invariant physical amplitudes. In this section, however, we consider only the VBF diagram. As we shall see later in section 5, after applying appropriate kinematical selection cuts, the VBF contribution can dominate the exact matrix elements.

Let us first define a common set of kinematical variables for the VBF subprocesses (2.1) generically as

$$\begin{aligned} a_1(k_1,\sigma_1) + a_2(k_2,\sigma_2) &\to a_3(k_3,\sigma_3) + a_4(k_4,\sigma_4) + V_1^*(q_1,\lambda_1) + V_2^*(q_2,\lambda_2) \\ &\to a_3(k_3,\sigma_3) + a_4(k_4,\sigma_4) + X(P,\lambda), \end{aligned} \tag{2.2}$$

where $a_{1,\cdots,4}$ stand for quarks or gluons (or even leptons in case of lepton-lepton or lepton-hadron collisions), and the four-momentum and the helicity of each particle are shown in parentheses; see also figure 2(a). The parton helicities take the values $\sigma_i/2$ for quarks or antiquarks and σ_i for gluons with $\sigma_i = \pm 1$, while the helicities of the off-shell vector-bosons take $\lambda_i = \pm 1, 0$.

The helicity amplitudes for the VBF processes (2.1) can generally be expressed as

$$\begin{aligned} \mathcal{M}^{\lambda}_{\sigma_1\sigma_3,\sigma_2\sigma_4} = \sum_{V_{1,2}} & J^{\mu_1'}_{V_1 a_1 a_3}(k_1,k_3;\sigma_1,\sigma_3)\, J^{\mu_2'}_{V_2 a_2 a_4}(k_2,k_4;\sigma_2,\sigma_4) \\ & \times D^{V_1}_{\mu_1'\mu_1}(q_1)\, D^{V_2}_{\mu_2'\mu_2}(q_2)\, \Gamma^{\mu_1\mu_2}_{X V_1 V_2}(q_1,q_2;\lambda)^*, \end{aligned} \tag{2.3}$$

JHEP07(2009)101

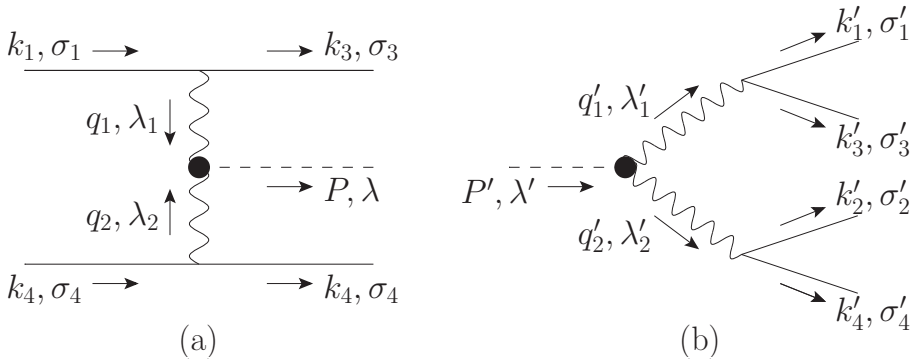

Figure 2. Schematic view of the subprocesses for (a) the X production with 2 jets via VBF, and (b) the X decay to 4 jets via a vector-boson pair. The four-momentum and the helicity of each particle are shown. The solid lines show either fermions or gluons.

where $J^{\mu}_{V_1 a_1 a_3}$ and $J^{\mu}_{V_2 a_2 a_4}$ are the external fermion or gluon currents, and the vector-boson propagators are

$$D^{V_i}_{\mu'\mu}(q_i) = \begin{cases} \Big(-g_{\mu'\mu} + \dfrac{q_{i\mu'} q_{i\mu}}{m^2_{V_i}} \Big) D_{V_i}(q_i^2) & \text{for } V_i = W,\, Z, \\ -g_{\mu'\mu}\, D_{V_i}(q_i^2) & \text{for } V_i = \gamma,\, g, \end{cases} \tag{2.4}$$

with the propagator factor $D_V(q^2) = (q^2 - m_V^2 + i m_V \Gamma_V)^{-1}$. Note that we choose the unitary-gauge propagator for the massive vector-bosons and the Feynman-gauge one for the massless vector-bosons ($m_{V_i} = 0$). The XVV vertex is expressed generically as $\Gamma^{\mu_1\mu_2}_{XV_1V_2}$, whose explicit forms are given in section 4.3.

Using the completeness relation for space-like vector-bosons ($q_i^2 < 0$)

$$-g_{\mu'\mu} + \frac{q_{i\mu'} q_{i\mu}}{q_i^2} = \sum_{\lambda_i = \pm, 0} (-1)^{\lambda_i + 1}\, \epsilon_{\mu'}(q_i, \lambda_i)^*\, \epsilon_{\mu}(q_i, \lambda_i), \tag{2.5}$$

and neglecting the terms which vanish due to current conservation

$$q_{i\mu} J^{\mu}_{V_i a_i a_{i+2}}(k_i, k_{i+2}; \sigma_i, \sigma_{i+2}) = 0, \tag{2.6}$$

the VBF helicity amplitudes (2.3) can be rewritten as the product of the two incoming current ($f \to fV^*$ or $g \to gV^*$) amplitudes and the off-shell VBF X production ($V^*V^* \to X$) amplitudes summed over the polarization of the intermediate vector-bosons

$$\mathcal{M}^{\lambda}_{\sigma_1\sigma_3,\sigma_2\sigma_4} = \sum_{V_{1,2}} D_{V_1}(q_1^2) D_{V_2}(q_2^2) \sum_{\lambda_{1,2}} \big(\mathcal{J}^{V_1}_{a_1 a_3}\big)^{\lambda_1}_{\sigma_1\sigma_3} \big(\mathcal{J}^{V_2}_{a_2 a_4}\big)^{\lambda_2}_{\sigma_2\sigma_4} \big(\mathcal{M}^{X}_{V_1V_2}\big)^{\lambda}_{\lambda_1\lambda_2}, \tag{2.7}$$

where

$$\big(\mathcal{J}^{V_i}_{a_i a_{i+2}}\big)^{\lambda_i}_{\sigma_i\sigma_{i+2}} = (-1)^{\lambda_i+1} J^{\mu}_{V_i a_i a_{i+2}}(k_i, k_{i+2}; \sigma_i, \sigma_{i+2})\, \epsilon_{\mu}(q_i, \lambda_i)^*, \tag{2.8}$$

$$\big(\mathcal{M}^{X}_{V_1V_2}\big)^{\lambda}_{\lambda_1\lambda_2} = \epsilon_{\mu_1}(q_1, \lambda_1)\, \epsilon_{\mu_2}(q_2, \lambda_2)\, \Gamma^{\mu_1\mu_2}_{XV_1V_2}(q_1, q_2; \lambda)^*. \tag{2.9}$$

JHEP07(2009)101

Aside from the summation of $V_{1,2}$, the VBF amplitudes (2.7) are generally the coherent sum of the nine amplitudes which have the different helicity combinations of the colliding vector-bosons. The explicit forms of the amplitudes (2.8) and (2.9) will be given in section 4.1 and 4.3, respectively. It is worth noting here that the current conservation (2.6), which ensures that the propagating vector-bosons have only the three vector-boson components, plays an essential role in deriving the above expressions, and that it is valid not only for currents made of massless fermions but also for those made of on-shell gluons.

In figure 2, we notice that the diagrams for (a) the X production with 2 jets via VBF and those for (b) the X decay into 4 jets via a vector-boson pair have identical topology, even though the intermediate vector-bosons are space-like for the production while they are time-like for the decay. They are related with each other by the crossing symmetry. Therefore, it may be useful to study the decay angular distributions and correlations in all the channels simultaneously.

We consider X decays into a (virtual) vector-boson pair which subsequently decay into $\ell\bar{\ell}$, $q\bar{q}$, or gg, similar to the Xjj productions via the VBF processes (2.1),

$$X \to V^{(*)}V^{(*)} \to (\ell\bar{\ell}/q\bar{q})(\ell\bar{\ell}/q\bar{q}) \qquad (V = W,\, Z,\, \gamma,\, g), \tag{2.10a}$$

$$X \to V^*V^* \to (q\bar{q})(gg) \qquad (V = g), \tag{2.10b}$$

$$X \to V^*V^* \to (gg)(gg) \qquad (V = g), \tag{2.10c}$$

and define a common set of kinematical variables as

$$\begin{aligned} X(P',\lambda') &\to V_1'^*(q_1',\lambda_1') + V_2'^*(q_2',\lambda_2') \\ &\to a_1'(k_1',\sigma_1') + a_3'(k_3',\sigma_3') + a_2'(k_2',\sigma_2') + a_4'(k_4',\sigma_4'), \end{aligned} \tag{2.11}$$

where the same notations for their momenta and helicities are used as in the production processes (2.2) except for primes ($'$); see also figure 2.

The decay helicity amplitudes can be expressed in the same way as the production amplitudes, while the completeness relation for time-like vector bosons has to be

$$-g_{\mu'\mu} + \frac{q_{i\mu'}' q_{i\mu}'}{q_i'^2} = \sum_{\lambda_i'=\pm,\,0} \epsilon_{\mu'}(q_i',\lambda_i')^*\, \epsilon_{\mu}(q_i',\lambda_i'). \tag{2.12}$$

We note that no extra sign factor for $\lambda_i' = 0$ is needed for $q_i'^2 > 0$. The outgoing fermion or gluon current ($V^* \to f\bar{f}$ or gg) amplitudes and the $X \to VV$ decay amplitudes, corresponding to eqs. (2.8) and (2.9) for the production, are given by

$$\left(\mathcal{J}'^{V_i'}_{a_i'a_{i+2}'}\right)^{\lambda_i'}_{\sigma_i'\sigma_{i+2}'} = \epsilon_\mu(q_i',\lambda_i')\, J'^{\mu}_{V_i'a_i'a_{i+2}'}(k_i',k_{i+2}';\sigma_i',\sigma_{i+2}'), \tag{2.13}$$

$$\left(\mathcal{M}'^{X}_{V_1'V_2'}\right)^{\lambda'}_{\lambda_1'\lambda_2'} = \Gamma^{\mu_1\mu_2}_{XV_1'V_2'}(q_1',q_2';\lambda')\, \epsilon_{\mu_1}(q_1',\lambda_1')^*\, \epsilon_{\mu_2}(q_2',\lambda_2')^*. \tag{2.14}$$

The helicity amplitudes for the X decay processes (2.10) can now be expressed as

$$\mathcal{M}'^{\lambda'}_{\sigma_1'\sigma_3',\sigma_2'\sigma_4'} = \sum_{V_{1,2}'} D_{V_1'}(q_1'^2) D_{V_2'}(q_2'^2) \sum_{\lambda_{1,2}'} \left(\mathcal{M}'^{X}_{V_1'V_2'}\right)^{\lambda'}_{\lambda_1'\lambda_2'} \left(\mathcal{J}'^{V_1'}_{a_1'a_3'}\right)^{\lambda_1'}_{\sigma_1'\sigma_3'} \left(\mathcal{J}'^{V_2'}_{a_2'a_4'}\right)^{\lambda_2'}_{\sigma_2'\sigma_4'}. \tag{2.15}$$

JHEP07(2009)101

Similar to the VBF production amplitudes (2.7), the decay amplitudes (2.15) are generally the sum of the nine amplitudes. We note our convention that the sign of the current amplitudes with the longitudinal polarization is different between the incoming and outgoing current amplitudes, (2.8) and (2.13), reflecting the difference between (2.5) and (2.12) for the spin-1 completeness relation.

For the sake of our later discussions, we give the complete amplitudes and the squared matrix elements for the subprocesses of the X plus n-jet production and its subsequent decay into n' jets. In the vicinity of the X resonance pole, the full amplitudes can be factorized into the X production amplitudes and its decay amplitudes, summed over the helicity of the X resonance. In the X rest frame, if we use the X polarization along the z-axis ($J_z = \lambda$) to express the production amplitudes and that of the decaying direction ($J_{z'} = \lambda'$) to express the decay amplitudes, the full amplitudes can be expressed as

$$\mathcal{M}_{\sigma_{1,\cdots,n+2};\sigma'_{1,\cdots,n'}} = \sum_{\lambda,\lambda'} \mathcal{M}^{\lambda}_{\sigma_{1,\cdots,n+2}}\, D_X(P^2)\, d^J_{\lambda,\lambda'}(\Theta)\, \mathcal{M}'^{\lambda'}_{\sigma'_{1,\cdots,n'}}, \tag{2.16}$$

where $D_X(P^2) = (P^2 - M^2 + iM\Gamma)^{-1}$ times the Wigner's d function $d^J_{\lambda,\lambda'}(\Theta)$ gives the X propagator in the X rest frame when the X spin is J and the initial and the final quantization axes have the opening angle Θ. For instance, for the $n = 0$ case the initial X polarization is $\lambda = \sigma_1 - \sigma_2$, while the final polarization is $\lambda' = \sigma'_1 - \sigma'_2$ for $n' = 2$. We derive the above expression explicitly for the $J = 2$ case in appendix B. The amplitudes for the scalar particle production and its decay processes have no Θ dependence, i.e. $d^{J=0}_{\lambda,\bar{\lambda}'}(\Theta) = d^0_{00}(\Theta) = 1$.

It is straightforward to obtain the polarization-summed squared matrix elements of the full production plus decay amplitudes (2.16),

$$\begin{aligned}\sum |\mathcal{M}|^2 &\equiv \sum_{\sigma_{1,\cdots,n+2}} \sum_{\sigma'_{1,\cdots,n'}} \left|\mathcal{M}_{\sigma_{1,\cdots,n+2};\sigma'_{1,\cdots,n'}}\right|^2 \\ &= \left|D_X(P^2)\right|^2 \sum_{\lambda,\lambda'} \sum_{\bar{\lambda},\bar{\lambda}'} \mathcal{P}^X_{\lambda\bar{\lambda}}\, d^J_{\lambda,\lambda'}(\Theta)\, d^J_{\bar{\lambda},\bar{\lambda}'}(\Theta)\, \mathcal{D}^X_{\lambda'\bar{\lambda}'}\end{aligned} \tag{2.17}$$

in terms of the production density matrix $\mathcal{P}^X_{\lambda\bar{\lambda}}$ and the decay density matrix $\mathcal{D}^X_{\lambda'\bar{\lambda}'}$;

$$\mathcal{P}^X_{\lambda\bar{\lambda}} = \sum_{\sigma_{1,\cdots,n+2}} \mathcal{M}^{\lambda}_{\sigma_{1,\cdots,n+2}} \left(\mathcal{M}^{\bar{\lambda}}_{\sigma_{1,\cdots,n+2}}\right)^*, \tag{2.18a}$$

$$\mathcal{D}^X_{\lambda'\bar{\lambda}'} = \sum_{\sigma'_{1,\cdots,n'}} \mathcal{M}'^{\lambda'}_{\sigma'_{1,\cdots,n'}} \left(\mathcal{M}'^{\bar{\lambda}'}_{\sigma'_{1,\cdots,n'}}\right)^*. \tag{2.18b}$$

Although eq. (2.17) applies only for parton-level subprocesses, one can easily generalize it to mixed case and apply it for any processes, including summation over different subprocesses and a product of the relevant parton distribution functions. We note that the density matrices together with the d functions have all information on the angular distributions of the final states.

JHEP07(2009)101

For the VBF processes (2.1) and for the X decays into a pair of vector bosons (2.10), the density matrices can be expressed as

$$\mathcal{P}^X_{\lambda\bar{\lambda}} = \sum_{V_{1,2}} \left|D_{V_1}(q_1^2) D_{V_2}(q_2^2)\right|^2 \sum_{\lambda_{1,2}} \sum_{\bar{\lambda}_{1,2}} \delta(\lambda_1 - \lambda_2 - \lambda)\, \delta(\bar{\lambda}_1 - \bar{\lambda}_2 - \bar{\lambda})\, \mathcal{P}^{\lambda_1\lambda_2}_{\bar{\lambda}_1\bar{\lambda}_2}, \tag{2.19a}$$

$$\mathcal{D}^X_{\lambda'\bar{\lambda}'} = \sum_{V'_{1,2}} \left|D_{V'_1}(q_1'^2) D_{V'_2}(q_2'^2)\right|^2 \sum_{\lambda'_{1,2}} \sum_{\bar{\lambda}'_{1,2}} \delta(\lambda'_1 - \lambda'_2 - \lambda')\, \delta(\bar{\lambda}'_1 - \bar{\lambda}'_2 - \bar{\lambda}')\, \mathcal{D}^{\lambda'_1\lambda'_2}_{\bar{\lambda}'_1\bar{\lambda}'_2}, \tag{2.19b}$$

in terms of the colliding or the decaying vector-boson polarization amplitudes, (2.7) or (2.15);

$$\mathcal{P}^{\lambda_1\lambda_2}_{\bar{\lambda}_1\bar{\lambda}_2} = \sum_{\sigma_{1,\cdots,4}} \left[\mathcal{J}_1{}^{\lambda_1}_{\sigma_1\sigma_3} \mathcal{J}_2{}^{\lambda_2}_{\sigma_2\sigma_4} \mathcal{M}_X{}^{\lambda}_{\lambda_1\lambda_2}\right] \left[\mathcal{J}_1{}^{\bar{\lambda}_1}_{\sigma_1\sigma_3} \mathcal{J}_2{}^{\bar{\lambda}_2}_{\sigma_2\sigma_4} \mathcal{M}_X{}^{\bar{\lambda}}_{\bar{\lambda}_1\bar{\lambda}_2}\right]^*, \tag{2.20a}$$

$$\mathcal{D}^{\lambda'_1\lambda'_2}_{\bar{\lambda}'_1\bar{\lambda}'_2} = \sum_{\sigma'_{1,\cdots,4}} \left[\mathcal{M}'_X{}^{\lambda'}_{\lambda'_1\lambda'_2} \mathcal{J}'_1{}^{\lambda'_1}_{\sigma'_1\sigma'_3} \mathcal{J}'_2{}^{\lambda'_2}_{\sigma'_2\sigma'_4}\right] \left[\mathcal{M}'_X{}^{\bar{\lambda}'}_{\bar{\lambda}'_1\bar{\lambda}'_2} \mathcal{J}'_1{}^{\bar{\lambda}'_1}_{\sigma'_1\sigma'_3} \mathcal{J}'_2{}^{\bar{\lambda}'_2}_{\sigma'_2\sigma'_4}\right]^*. \tag{2.20b}$$

3 Kinematics

In this section, we define kinematical variables for the production of the heavy particle X (2.2) and its decay (2.11). The angular configuration of the particles defined below is summarized in figure 3. It must be noted again that the same notations except for primes ($'$) are used both for the production and the decay.

First of all, we note the relations between the momenta by the momentum conservation.

$$q_1 + q_2 = P = P' = q'_1 + q'_2 \tag{3.1}$$

with $q_i = k_i - k_{i+2}$ and $q'_i = k'_i + k'_{i+2}$. On-shell conditions for the external particles and the partonic center-of-mass (CM) energy are

$$k_i^2 = k_{i+2}^2 = k_i'^2 = k_{i+2}'^2 = 0, \quad P^2 = P'^2 = M^2, \quad \text{and} \quad \hat{s} = (k_1 + k_2)^2, \tag{3.2}$$

while the intermediate vector-bosons are off-shell;

$$q_i^2 < 0, \quad q_i'^2 > 0. \tag{3.3}$$

We would like to express the $VV \to X$ production amplitudes (2.9) and the $X \to VV$ decay amplitudes (2.14) in the X rest frame where the colliding or decaying (virtual) vector-boson momenta are chosen as the polar axis, along which their helicities are defined. Because the helicities are invariant under the boost along the polar axis, we evaluate the vector-boson emission amplitudes in the Breit frames, $q_{1z} = \sqrt{-q_1^2}$ or $q_{2z} = -\sqrt{-q_2^2}$, and the vector-boson decay amplitudes in their rest frames, $q_1'^0 = \sqrt{q_1'^2}$ or $q_2'^0 = \sqrt{q_2'^2}$.

For the X + 2-jet production process via VBF (2.2), we parametrize the momenta of the quarks, antiquarks or gluons of the incoming currents in the Breit frame as follows:

JHEP07(2009)101

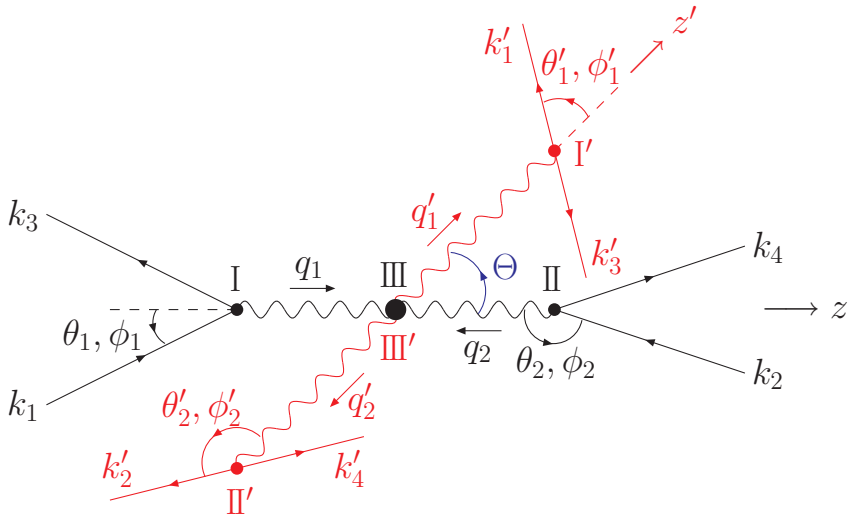

Figure 3. The momentum and angular configuration of the particles in the q_1 and q_2 Breit frame, (I) and (II), and the VBF frame (III) for the production; in the q_1' and q_2' rest frame, (I′) and (II′), and the X rest frame (III′) for the decay.

(I) the q_1 Breit frame

$$\begin{aligned} q_1^\mu &= k_1^\mu - k_3^\mu = (0,\, 0,\, 0,\, Q_1), \\ k_1^\mu &= \frac{Q_1}{2\cos\theta_1}(1,\, \sin\theta_1\cos\phi_1,\, \sin\theta_1\sin\phi_1,\, \cos\theta_1), \\ k_3^\mu &= \frac{Q_1}{2\cos\theta_1}(1,\, \sin\theta_1\cos\phi_1,\, \sin\theta_1\sin\phi_1,\, -\cos\theta_1), \end{aligned} \tag{3.4}$$

where $Q_1 = \sqrt{-q_1^2}$, $0 < \theta_1 < \pi/2$ and $0 < \phi_1 < 2\pi$.

(II) the q_2 Breit frame

$$\begin{aligned} q_2^\mu &= k_2^\mu - k_4^\mu = (0,\, 0,\, 0,\, -Q_2), \\ k_2^\mu &= -\frac{Q_2}{2\cos\theta_2}(1,\, \sin\theta_2\cos\phi_2,\, \sin\theta_2\sin\phi_2,\, \cos\theta_2), \\ k_4^\mu &= -\frac{Q_2}{2\cos\theta_2}(1,\, \sin\theta_2\cos\phi_2,\, \sin\theta_2\sin\phi_2,\, -\cos\theta_2), \end{aligned} \tag{3.5}$$

where $Q_2 = \sqrt{-q_2^2}$, $\pi/2 < \theta_2 < \pi$ and $0 < \phi_2 < 2\pi$.

The momenta of the t-channel intermediate vector-bosons are chosen along the z-axis, and the coordinate system where the vector boson has a positive (negative) momentum along the z-axis is labeled as 1 (2). In practice, we always denote by k_1 the parton momentum in the colliding proton with $p_z = \sqrt{s}/2$, while k_2 denotes the parton momentum in the other proton (or anti-proton) with $p_z = -\sqrt{s}/2$, in the laboratory frame. This agrees with the above definition whenever the VBF approximation to the full amplitude is valid. The polar angles θ_1 and θ_2 are measured from the common positive z-axis; see also figure 3.

JHEP07(2009)101

By a boost along the z-axis, each Breit frame can be transformed to the rest frame of the heavy particle, referred to as the VBF frame:

(III) the VBF frame

$$\begin{aligned}
q_1^\mu + q_2^\mu = P^\mu = P'^\mu = q_1'^\mu + q_2'^\mu &= (M,\, 0,\, 0,\, 0),\\
q_1^\mu &= \frac{M}{2}\left(1 - \frac{Q_1^2 - Q_2^2}{M^2},\, 0,\, 0,\, \beta\right),\\
q_2^\mu &= \frac{M}{2}\left(1 - \frac{Q_2^2 - Q_1^2}{M^2},\, 0,\, 0,\, -\beta\right),\\
q_1'^\mu &= \frac{M}{2}\left(1 + \frac{Q_1'^{\,2} - Q_2'^{\,2}}{M^2},\, \beta' \sin\Theta,\, 0,\, \beta' \cos\Theta\right),\\
q_2'^\mu &= \frac{M}{2}\left(1 + \frac{Q_2'^{\,2} - Q_1'^{\,2}}{M^2},\, -\beta' \sin\Theta,\, 0,\, -\beta' \cos\Theta\right),
\end{aligned} \tag{3.6}$$

where $Q_i' = \sqrt{q_i'^2}$, $\beta = \bar{\beta}\big(-\frac{Q_1^2}{M^2}, -\frac{Q_2^2}{M^2}\big)$ and $\beta' = \bar{\beta}\big(\frac{Q_1'^{\,2}}{M^2}, \frac{Q_2'^{\,2}}{M^2}\big)$ with $\bar{\beta}(a,b) \equiv (1 + a^2 + b^2 - 2a - 2b - 2ab)^{1/2}$, and Θ is the angle between the production axis (z-axis) and the decay axis (z'-axis). The boost factor along the z-axis from each Breit frame to the VBF frame is, respectively,

$$\beta_1 = \left(1 - \frac{Q_1^2 - Q_2^2}{M^2}\right)/\beta, \tag{3.7a}$$

$$\beta_2 = -\left(1 - \frac{Q_2^2 - Q_1^2}{M^2}\right)/\beta. \tag{3.7b}$$

We note that, when the produced particle X decays into visible particles and its momentum is reconstructed together with those of the two tagging jets, the Breit frames can in principle be reconstructed in experiments.

For the X decays into 4 jets via a (virtual) vector-boson pair (2.11), the momenta of the time-like vector-bosons are measured along the z'-axis in the X rest frame:

(III$'$) the X rest frame

$$\begin{aligned}
q_1^\mu + q_2^\mu = P^\mu = P'^\mu = q_1'^\mu + q_2'^\mu &= (M,\, 0,\, 0,\, 0),\\
q_1^\mu &= \frac{M}{2}\left(1 - \frac{Q_1^2 - Q_2^2}{M^2},\, -\beta \sin\Theta,\, 0,\, \beta \cos\Theta\right),\\
q_2^\mu &= \frac{M}{2}\big(g1 - \frac{Q_2^2 - Q_1^2}{M^2},\, \beta \sin\Theta,\, 0,\, -\beta \cos\Theta\right),\\
q_1'^\mu &= \frac{M}{2}\left(1 + \frac{Q_1'^{\,2} - Q_2'^{\,2}}{M^2},\, 0,\, 0,\, \beta'\right),\\
q_2'^\mu &= \frac{M}{2}\left(1 + \frac{Q_2'^{\,2} - Q_1'^{\,2}}{M^2},\, 0,\, 0,\, -\beta'\right),
\end{aligned} \tag{3.8}$$

which is obtained from the VBF frame (3.6) by the rotation with the angle $(-\Theta)$ about the y-axis.

For the outgoing fermions and gluons, their momenta are parametrized in the rest frames of the time-like vector-bosons as follows;

(I′) the q_1' rest frame:

$$\begin{aligned} q_1'^{\,\mu} &= k_1'^{\,\mu} + k_3'^{\,\mu} = (Q_1',\, 0,\, 0,\, 0), \\ k_1'^{\,\mu} &= \frac{Q_1'}{2}(1,\, \sin\theta_1' \cos\phi_1',\, \sin\theta_1' \sin\phi_1',\, \cos\theta_1'), \\ k_3'^{\,\mu} &= \frac{Q_1'}{2}(1,\, -\sin\theta_1' \cos\phi_1',\, -\sin\theta_1' \sin\phi_1',\, -\cos\theta_1'), \end{aligned} \tag{3.9}$$

(II′) the q_2' rest frame:

$$\begin{aligned} q_2'^{\,\mu} &= k_2'^{\,\mu} + k_4'^{\,\mu} = (Q_2',\, 0,\, 0,\, 0), \\ k_2'^{\,\mu} &= \frac{Q_2'}{2}(1,\, \sin\theta_2' \cos\phi_2',\, \sin\theta_2' \sin\phi_2',\, \cos\theta_2'), \\ k_4'^{\,\mu} &= \frac{Q_2'}{2}(1,\, -\sin\theta_2' \cos\phi_2',\, -\sin\theta_2' \sin\phi_2',\, -\cos\theta_2'), \end{aligned} \tag{3.10}$$

where $0 < \theta_i' < \pi$ and $0 < \phi_i' < 2\pi$. In the X rest frame, the q_1' momentum is chosen along the z'-axis, and the q_2' momentum along the negative z'-axis. The polar (z'-)axis and the y-axis normal to the scattering plane are chosen common to all the three frames for the decay chain, III′, I′ and II′, which are related with each other by a boost along the z'-axis; see also figure 3. For instance, both $\cos\theta_1' = 1$ in (3.9) and $\cos\theta_2' = 1$ in (3.10) denote the momentum along the z'-axis direction, and hence the a_1' momentum (k_1') is along the V_1' momentum while the a_2' momentum (k_2') is anti-parallel to the V_2' momentum in the X rest frame. The boost factor along the z'-axis from each vector-boson rest frame to the X rest frame is, respectively,

$$\beta_1' = \beta' \Big/ \left(1 + \frac{{Q_1'}^2 - {Q_2'}^2}{M^2}\right), \tag{3.11a}$$

$$\beta_2' = -\beta' \Big/ \left(1 + \frac{{Q_2'}^2 - {Q_1'}^2}{M^2}\right). \tag{3.11b}$$

4 Helicity amplitudes

As we have shown in section 2, the VBF helicity amplitudes (2.7) can be expressed by the product of the two incoming current amplitudes and the $VV \to X$ fusion amplitudes. Similarly, the decay helicity amplitudes (2.15) can be given by the product of the $X \to VV$ decay amplitudes and the two outgoing current amplitudes. In this section, using the helicity amplitude technique [36] and the kinematical variables defined in the previous section, we present all the helicity amplitudes explicitly for the fermion currents, the gluon currents, and the off-shell VBF vertices, respectively. We also discuss the relation between the off-shell vector-boson current amplitudes and the standard parton splitting amplitudes [37].

JHEP07(2009)101

4.1 Current amplitudes

Let us start with the helicity amplitudes for the incoming fermion currents ($f \to fV^*$) in the X production process, $\big(\mathcal{J}^{V_i}_{a_i a_{i+2}}\big)^{\lambda_i}_{\sigma_i\sigma_{i+2}}$ in eq. (2.8). The fermion and antifermion currents are given by

$$J^{\mu}_{Vff'}(k_i,k_{i+2};\sigma_i,\sigma_{i+2}) = g^{Vff'}_{\sigma_i}\,\bar{u}_{f'}(k_{i+2},\sigma_{i+2})\,\gamma^{\mu}\,u_f(k_i,\sigma_i), \tag{4.1}$$

$$J^{\mu}_{V\bar{f}\bar{f}'}(k_i,k_{i+2};\sigma_i,\sigma_{i+2}) = g^{Vff'}_{-\sigma_i}\,\bar{v}_f(k_i,\sigma_i)\,\gamma^{\mu}\,v_{f'}(k_{i+2},\sigma_{i+2}). \tag{4.2}$$

Non-vanishing couplings in the standard model (SM) are

$$\begin{aligned} g^{\gamma ff}_{\pm} &= eQ_f, & g^{gff}_{\pm} &= g_s t^a,\\ g^{Zff}_{+} &= -g_Z Q_f \sin^2\theta_W, & g^{Zff}_{-} &= g_Z[T_{3f} - Q_f\sin^2\theta_W],\\ g^{Wu_id_j}_{-} &= \big(g^{Wd_ju_i}_{-}\big)^* = \big(g_W/\sqrt{2}\big)V_{ij}, \end{aligned} \tag{4.3}$$

where $e = \sqrt{4\pi\alpha}$ is the magnitude of the electron charge, $g_s = \sqrt{4\pi\alpha_s}$ is the QCD coupling constant, $e = g_W\sin\theta_W = g_Z\sin\theta_W\cos\theta_W$, t^a is the SU(3) color matrix, and V_{ij} denotes the Cabibbo-Kobayashi-Maskawa (CKM) matrix element. Using the kinematical variables defined in the previous section and contracting the above current with the final-state polarization vector $\epsilon^{\mu}(q_i,\lambda_i)^*$, we can obtain the helicity amplitudes explicitly for all the helicity combinations; see eq. (2.8). For our analytical calculations, we use the HELAS convention [38] for the spinors. For the virtual vector bosons with space-like momentum, $q_i^2 = -Q_i^2 < 0$, we define the longitudinal polarization vectors as

$$\epsilon^{\mu}(q_i,\lambda_i=0) = \frac{q_i^0}{Q_i|\vec{q}_i|}\,(|\vec{q}_i|^2/q_i^0,\,\vec{q}_i\,) \tag{4.4}$$

with $Q_i = \sqrt{|(q_i^0)^2 - |\vec{q}_i|^2|}$. By choosing the transverse polarization vectors $\epsilon^{\mu}(q_i,\lambda_i=\pm)$ about the $\vec{q}_i$ axis, the identity (2.5) holds.

Here, for notational convenience, we define the reduced current amplitudes $\hat{\mathcal{J}}_i{}^{\lambda_i}_{\sigma_i\sigma_{i+2}}$ as

$$\big(\mathcal{J}^{V_i}_{a_i a_{i+2}}\big)^{\lambda_i}_{\sigma_i\sigma_{i+2}} = \sqrt{2}\,g^{V_i a_i a_{i+2}}_{\sigma_i} Q_i\,\hat{\mathcal{J}}_i{}^{\lambda_i}_{\sigma_i\sigma_{i+2}}. \tag{4.5}$$

In table 1(top), the reduced helicity amplitudes for the incoming fermion currents, $\hat{\mathcal{J}}_1{}^{\lambda_1}_{\sigma_1\sigma_3}$ ($f_{\sigma_1} \to f_{\sigma_3}V^*_{\lambda_1}$), are shown in the q_1 Breit frame (3.4), or the frame I in figure 3. The following features of the amplitudes are worth noting: (i) The reduced amplitudes for the antiquark currents are the same as those for the quark currents. (ii) Parity transformation gives the relation $\hat{\mathcal{J}}_1{}^{\lambda_1}_{\sigma_1,\sigma_3} = (-1)^{\lambda_1}(\hat{\mathcal{J}}_1{}^{-\lambda_1}_{-\sigma_1,-\sigma_3})^*$. (iii) The quark masses are neglected (eq. (3.2)), and hence the helicity-flip amplitudes $\hat{\mathcal{J}}_1{}^{\lambda_1}_{\sigma,-\sigma}$ are zero due to the chirality conservation. (iv) The amplitudes $\hat{\mathcal{J}}_2$ are related to $\hat{\mathcal{J}}_1$ by

$$\hat{\mathcal{J}}_2{}^{\lambda_2}_{\sigma_2\sigma_4}(\theta_2,\phi_2) = (-1)^{\lambda_2+1}\hat{\mathcal{J}}_1{}^{-\lambda_2}_{\sigma_2\sigma_4}(\theta_2,\phi_2). \tag{4.6}$$

(v) The $1/\cos\theta_1$ dependence comes from the common factor of the four-momentum in the q_1 Breit frame (3.4), and this gives rise to the enhancement of the amplitudes when

$\hat{\mathcal{J}}_{1\,\sigma_1\sigma_3}^{\lambda_1}(f_{\sigma_1} \to f_{\sigma_3} V_{\lambda_1}^*)$		$[\cos\theta_1 \to z_1/(2-z_1)]$
$\hat{\mathcal{J}}_{1\,++}^{+} = -\big(\hat{\mathcal{J}}_{1\,--}^{-}\big)^*$	$\dfrac{1}{2\cos\theta_1}(1+\cos\theta_1)\,e^{-i\phi_1}$	$\dfrac{1}{z_1}\,e^{-i\phi_1}$
$\hat{\mathcal{J}}_{1\,++}^{0} = \hat{\mathcal{J}}_{1\,--}^{0}$	$-\dfrac{1}{\sqrt{2}\cos\theta_1}\sin\theta_1$	$-\dfrac{\sqrt{2(1-z_1)}}{z_1}$
$\hat{\mathcal{J}}_{1\,++}^{-} = -\big(\hat{\mathcal{J}}_{1\,--}^{+}\big)^*$	$-\dfrac{1}{2\cos\theta_1}(1-\cos\theta_1)\,e^{i\phi_1}$	$-\dfrac{1-z_1}{z_1}\,e^{i\phi_1}$
$\hat{\mathcal{J}}_{1\,+-}^{\lambda_1} = \hat{\mathcal{J}}_{1\,-+}^{\lambda_1}$	0	0
$\hat{\mathcal{J}}'^{\lambda_1'}_{1\,\sigma_1'\sigma_3'}(V_{\lambda_1'}^* \to f_{\sigma_1'}\bar{f}_{\sigma_3'})$		$[\cos\theta_1' \to 2z_1' - 1]$
$\hat{\mathcal{J}}'^{+}_{1\,+-} = -\big(\hat{\mathcal{J}}'^{-}_{1\,-+}\big)^*$	$\dfrac{1}{2}(1+\cos\theta_1')\,e^{i\phi_1'}$	$z_1'\,e^{i\phi_1'}$
$\hat{\mathcal{J}}'^{0}_{1\,+-} = \hat{\mathcal{J}}'^{0}_{1\,-+}$	$\dfrac{1}{\sqrt{2}}\sin\theta_1'$	$\sqrt{2z_1'(1-z_1')}$
$\hat{\mathcal{J}}'^{-}_{1\,+-} = -\big(\hat{\mathcal{J}}'^{+}_{1\,-+}\big)^*$	$\dfrac{1}{2}(1-\cos\theta_1')\,e^{-i\phi_1'}$	$(1-z_1')\,e^{-i\phi_1'}$
$\hat{\mathcal{J}}'^{\lambda_1'}_{1\,++} = \hat{\mathcal{J}}'^{\lambda_1'}_{1\,--}$	0	0

Table 1. The reduced helicity amplitudes for the off-shell vector-boson currents: the incoming fermion currents $\hat{\mathcal{J}}_{1\,\sigma_1\sigma_3}^{\lambda_1}(f \to fV^*)$ in the Breit frame (top), and the outgoing fermion currents $\hat{\mathcal{J}}'^{\lambda_1'}_{1\,\sigma_1'\sigma_3'}(V^* \to f\bar{f})$ in the vector-boson rest frame (bottom). In the third column the splitting amplitudes are also shown in the collinear limit, where $z_1^{(\prime)}$ is the energy fraction of the initial particle.

$\cos\theta_1$ approaches zero. This singularity simply reflects the well-known soft singularity in the laboratory frame, and will be discussed further in section 4.2. (vi) The transverse currents $\hat{\mathcal{J}}^{\pm}$ have opposite phases with each other in terms of the azimuthal angle, while the longitudinal currents $\hat{\mathcal{J}}^0$ do not have the azimuthal angle dependence.

Next, for comparison, we consider the helicity amplitudes for the outgoing fermion currents $(V^* \to f\bar{f})$ in the X decay process, $\big(\mathcal{J}'^{\,V_i'}_{a_i'a_{i+2}'}\big)^{\lambda_i'}_{\sigma_i'\sigma_{i+2}'}$ in eq. (2.13). The fermion currents in which the time-like vector-bosons decay into $\ell\bar{\ell}$ or $q\bar{q}$ are given by

$$J'^{\mu}_{Vf\bar{f}'}(k_i', k_{i+2}'; \sigma_i', \sigma_{i+2}') = g_{\sigma_i'}^{Vff'}\,\bar{u}_f(k_i', \sigma_i')\,\gamma^{\mu}\,v_{f'}(k_{i+2}', \sigma_{i+2}'). \tag{4.7}$$

The reduced amplitudes for the outgoing currents, defined as in eq. (4.5),

$$\big(\mathcal{J}'^{\,V_i'}_{a_i'a_{i+2}'}\big)^{\lambda_i'}_{\sigma_i'\sigma_{i+2}'} = \sqrt{2}\,g_{\sigma_i'}^{V_i'a_i'a_{i+2}'}Q_i'\,\hat{\mathcal{J}}'^{\lambda_i'}_{i\,\sigma_i'\sigma_{i+2}'}, \tag{4.8}$$

can be obtained by contracting the current (4.7) with the initial-state polarization vector $\epsilon^{\mu}(q_i', \lambda_i')$; see eq. (2.13).

In table 1(bottom), the reduced helicity amplitudes for the outgoing fermion currents, $\hat{\mathcal{J}}'^{\lambda_1'}_{1\,\sigma_1'\sigma_3'}(V_{\lambda_1'}^* \to f_{\sigma_1'}\bar{f}_{\sigma_3'})$, are shown in the q_1' rest frame (3.9), or the frame I′ in figure 3. The amplitudes have similar features to the incoming current amplitudes in table 1(top). It is worth noting that not only the s-channel amplitudes $\hat{\mathcal{J}}'^{\lambda_1'}_{1\,\sigma_1'\sigma_3'}(V^* \to f\bar{f})$ but also the

JHEP07(2009)101

t-channel ones $\hat{\mathcal{J}}_{1\sigma_1\sigma_3}^{\lambda_1}(f \to fV^*)$ can be expressed by the same $J = 1$ d functions as

$$\hat{\mathcal{J}}_{1\sigma_1\sigma_3}^{\lambda_1}(f \to fV^*) \propto d^1_{\lambda_1,\,\sigma_1+\sigma_3}(\theta_1), \tag{4.9}$$

$$\hat{\mathcal{J}}'^{\lambda'_1}_{1\sigma'_1\sigma'_3}(V^* \to f\bar{f}) \propto d^1_{\lambda'_1,\,\sigma'_1-\sigma'_3}(\theta'_1). \tag{4.10}$$

The different points from the incoming current amplitudes are the following: (i) There is no $1/\cos\theta_1$ factor. (ii) The phases have opposite signs, reflecting the wavefunctions of the incoming and outgoing vector-bosons. (iii) The same-helicity amplitudes $\hat{\mathcal{J}}'^{\lambda'_1}_{1\sigma',\sigma'}$ are zero, which correspond to the chirality-flip amplitudes. (iv) The amplitudes $\hat{\mathcal{J}}'_2$ are given by

$$\hat{\mathcal{J}}'^{\lambda'_2}_{2\sigma'_2\sigma'_4}(\theta'_2,\phi'_2) = -\hat{\mathcal{J}}'^{-\lambda'_2}_{1\sigma'_2\sigma'_4}(\theta'_2,\phi'_2). \tag{4.11}$$

It is worth pointing out here that the list of the current amplitudes in table 1 is useful not only for hadron colliders but also for e^+e^-, ep and $\gamma\gamma$ colliders.

Turning now to the gluon current amplitudes, the incoming gluon currents in the X production process, $g \to gV^*$, where V^* is a virtual gluon, are given by

$$\begin{aligned} J^{\mu}_{Vgg}(k_i,k_{i+2};\sigma_i,\sigma_{i+2}) &= g_s f^{abc}\,\epsilon^b_\alpha(k_i,\sigma_i)\,\epsilon^c_\beta(k_{i+2},\sigma_{i+2})^* \\ &\times\big[-g^{\alpha\beta}(k_i+k_{i+2})^\mu - g^{\beta\mu}(-k_{i+2}+q_i)^\alpha - g^{\mu\alpha}(-q_i-k_i)^\beta\big], \end{aligned} \tag{4.12}$$

where f^{abc} is the structure constant of the SU(3) group. Similar to the fermion currents, the reduced amplitudes are defined as

$$\begin{aligned} \big(\mathcal{J}^V_{gg}\big)^{\lambda_i}_{\sigma_i\sigma_{i+2}} &= (-1)^{\lambda_i+1} J^{\mu}_{Vgg}(k_i,k_{i+2};\sigma_i,\sigma_{i+2})\,\epsilon_\mu(q_i,\lambda_i)^* \\ &= \sqrt{2}\,g_s f^{abc}\,Q_i\,\hat{\mathcal{J}}_{i\sigma_i\sigma_{i+2}}^{\lambda_i}. \end{aligned} \tag{4.13}$$

For the polarization vectors of the external gluons in the amplitude (4.13), we adopt a common light-cone gauge, $n_i^\mu = (1, -\vec{q}_i/|\vec{q}_i|)$, which satisfy

$$n_i\cdot\epsilon(k_i,\sigma_i) = n_i\cdot\epsilon(k_{i+2},\sigma_{i+2}) = n_i^2 = 0, \quad n_i\cdot k_i \neq 0, \quad n_i\cdot k_{i+2} \neq 0. \tag{4.14}$$

It should be noted that these gauge-fixing vectors are boost invariant along the current momentum directions, in particular between the Breit frames of I and II for $i = 1$ and 2, respectively, and the collision CM frame III.

By the crossing symmetry, the outgoing gluon currents in the X decay process, $V^* \to gg$, are obtained by making the replacements in eq. (4.12): $k_i \to -k'_i$, $k_{i+2} \to k'_{i+2}$, $q_i \to -q'_i$, and $\epsilon_\alpha \to \epsilon^*_\alpha$.

In table 2, we present the reduced helicity amplitudes for the incoming gluon currents, $\hat{\mathcal{J}}_{1\sigma_1\sigma_3}^{\lambda_1}(g_{\sigma_1} \to g_{\sigma_3}V^*_{\lambda_1})$, in the q_1 Breit frame (top), and for the outgoing gluon currents, $\hat{\mathcal{J}}'^{\lambda'_1}_{1\sigma'_1\sigma'_3}(V^*_{\lambda'_1} \to g_{\sigma'_1}g_{\sigma'_3})$, in the q'_1 rest frame (bottom). The derivations are straightforward as in the fermion case and the amplitudes have similar properties to those for fermions in table 1. However, the results for the gluon currents are more involved. The incoming amplitudes $\hat{\mathcal{J}}_2$ for the helicity-conserved currents ($\sigma_2 = \sigma_4$) are given by eq. (4.6), while the outgoing ones $\hat{\mathcal{J}}'_2$ for the opposite-helicity currents ($\sigma'_2 = -\sigma'_4$) are obtained by

$$\hat{\mathcal{J}}'^{\lambda'_2}_{2\sigma'_2\sigma'_4}(\theta'_2,\phi'_2) = \hat{\mathcal{J}}'^{-\lambda'_2}_{1\sigma'_2\sigma'_4}(\theta'_2,\phi'_2). \tag{4.15}$$

JHEP07(2009)101

$\hat{\mathcal{J}}_{1\,\sigma_1\sigma_3}^{\lambda_1}(g_{\sigma_1} \to g_{\sigma_3} V_{\lambda_1}^*)$		$[\cos\theta_1 \to z_1/(2-z_1)]$
$\hat{\mathcal{J}}_{1\,++}^{+} = -\big(\hat{\mathcal{J}}_{1\,--}^{-}\big)^*$	$\dfrac{1}{2\sin\theta_1\cos\theta_1}(1+\cos\theta_1)^2\, e^{-i\phi_1}$	$\dfrac{1}{z_1\sqrt{1-z_1}}\, e^{-i\phi_1}$
$\hat{\mathcal{J}}_{1\,++}^{0} = \hat{\mathcal{J}}_{1\,--}^{0}$	$-\dfrac{1}{\sqrt{2}\cos\theta_1}$	$-\dfrac{2-z_1}{\sqrt{2}\,z_1}$
$\hat{\mathcal{J}}_{1\,++}^{-} = -\big(\hat{\mathcal{J}}_{1\,--}^{+}\big)^*$	$-\dfrac{1}{2\sin\theta_1\cos\theta_1}(1-\cos\theta_1)^2\, e^{i\phi_1}$	$-\dfrac{(1-z_1)^2}{z_1\sqrt{1-z_1}}\, e^{i\phi_1}$
$\hat{\mathcal{J}}_{1\,+-}^{+} = -\big(\hat{\mathcal{J}}_{1\,-+}^{-}\big)^*$	$-\dfrac{2}{\tan\theta_1}\, e^{i\phi_1}$	$-\dfrac{z_1}{\sqrt{1-z_1}}\, e^{i\phi_1}$
$\hat{\mathcal{J}}_{1\,+-}^{0/-} = \hat{\mathcal{J}}_{1\,-+}^{0/+}$	0	0
$\hat{\mathcal{J}}'^{\lambda_1'}_{1\,\sigma_1'\sigma_3'}(V_{\lambda_1'}^* \to g_{\sigma_1'} g_{\sigma_3'})$		$[\cos\theta_1' \to 2z_1' - 1]$
$\hat{\mathcal{J}}_{1\,+-}'^{+} = -\big(\hat{\mathcal{J}}_{1\,-+}'^{-}\big)^*$	$-\dfrac{1}{2\sin\theta_1'}(1+\cos\theta_1')^2\, e^{i\phi_1'}$	$-\dfrac{z_1'^{\,2}}{\sqrt{z_1'(1-z_1')}}\, e^{i\phi_1'}$
$\hat{\mathcal{J}}_{1\,+-}'^{0} = \hat{\mathcal{J}}_{1\,-+}'^{0}$	$-\dfrac{1}{\sqrt{2}}\cos\theta_1'$	$-\dfrac{2z_1'-1}{\sqrt{2}}$
$\hat{\mathcal{J}}_{1\,+-}'^{-} = -\big(\hat{\mathcal{J}}_{1\,-+}'^{+}\big)^*$	$\dfrac{1}{2\sin\theta_1'}(1-\cos\theta_1')^2\, e^{-i\phi_1'}$	$\dfrac{(1-z_1')^2}{\sqrt{z_1'(1-z_1')}}\, e^{-i\phi_1'}$
$\hat{\mathcal{J}}_{1\,++}'^{+} = -\big(\hat{\mathcal{J}}_{1\,--}'^{-}\big)^*$	$\dfrac{2}{\sin\theta_1'}\, e^{-i\phi_1'}$	$\dfrac{1}{\sqrt{z_1'(1-z_1')}}\, e^{-i\phi_1'}$
$\hat{\mathcal{J}}_{1\,++}'^{0/-} = \hat{\mathcal{J}}_{1\,--}'^{0/+}$	0	0

Table 2. The same as table 1, but for the gluon currents, $g \to gV^*$ (top) and $V^* \to gg$ (bottom), where V^* is an off-shell gluon.

Unlike the fermion current amplitudes, some of the helicity-flip amplitudes ($\sigma_1 = -\sigma_3$) for the incoming currents and the same-helicity amplitudes ($\sigma_1' = \sigma_3'$) for the outgoing currents are nonzero, and the amplitudes $\hat{\mathcal{J}}_2^{(\prime)}$ are given by

$$\hat{\mathcal{J}}_{2\;\sigma_2^{(\prime)}\sigma_4^{(\prime)}}^{(\prime)\,\lambda_2^{(\prime)}}(\theta_2^{(\prime)}, \phi_2^{(\prime)}) = -\hat{\mathcal{J}}_{1\;\sigma_2^{(\prime)}\sigma_4^{(\prime)}}^{(\prime)\,\lambda_2^{(\prime)}}(\theta_2^{(\prime)}, \phi_2^{(\prime)}). \tag{4.16}$$

Furthermore, in addition to the singularity of the amplitudes at $\cos\theta_1 = 0$, which appears also in the incoming fermion amplitudes in table 1(top), the singularity at $\sin\theta_1^{(\prime)} = 0$, or $\cos\theta_1^{(\prime)} = 1$ also exists; see more discussions in section 4.2. It must be stressed here that the phase dependence of the gluonic currents and that of the fermionic currents are very similar, $e^{-i\lambda_1\phi_1}$ or $e^{i\lambda_1'\phi_1'}$ when the gluon helicity is conserved ($q_i^2 < 0$) or flipped ($q_i'^2 > 0$) as in the fermionic case. These phases lead to the azimuthal angle correlations of the jets, as we will show later.

4.2 Relation to the splitting amplitudes

Before turning to the XVV amplitudes, it may be valuable to discuss the off-shell vector-boson current amplitudes from a different point of view, parton branching description [37], where the outgoing particles are emitted collinearly.

JHEP07(2009)101

To begin with, we consider the incoming current amplitudes ($f \to fV^*$ or $g \to gV^*$). Let z be the energy fraction of the initial parton that is carried off by the space-like vector-boson. In the VBF frame (3.6), the energy fraction $z_1 = q_1^0/k_1^0$ is written in terms of $\cos\theta_1$ defined in the q_1 Breit frame (3.4) and the boost factor β_1 in eq. (3.7a) as

$$z_1 = \frac{q_1^0}{k_1^0} = \frac{2\beta_1 \cos\theta_1}{1+\beta_1\cos\theta_1}. \tag{4.17}$$

Taking the $\beta_1 = 1$ limit, where the space-like vector-boson becomes on-shell and collinear with the final parton, we obtain the simple relation between the Breit-frame angle $\cos\theta_1$ and the energy fraction z_1 as

$$\cos\theta_1 = \frac{z_1}{\beta_1(2-z_1)} \overset{\beta_1=1}{\longrightarrow} \frac{z_1}{2-z_1}. \tag{4.18}$$

In the third column in tables 1(top) and 2(top), using the above relation (4.18) in the $\beta_1 = 1$ limit, or in the collinear limit, the helicity amplitudes for the incoming fermion and gluon currents are rewritten as splitting amplitudes with appropriate phases. These formulae may give us clear explanation for the origin of the singularities of the amplitudes which we encountered in the previous section. We see from table 1(top) for the incoming fermion splitting that the amplitudes are enhanced at $z_1 \to 0$, where the vector boson becomes soft. On the other hand, for the $g \to gV^*$ splitting in table 2(top), the enhancements of the amplitudes at $z_1 \to 0$ and 1 are associated with the soft emissions of the space-like gluon and the outgoing jet gluon, respectively.

Next, we consider the outgoing current amplitudes ($V^* \to f\bar{f}$ or gg). Here, we define a fraction z' as the energy transferred from the time-like vector-boson to the outgoing fermion or gluon. In the X rest frame (3.8),

$$z_1' = \frac{k_1'^{\,0}}{q_1'^{\,0}} = \frac{1}{2\beta_1'}(1+\beta_1'\cos\theta_1'), \tag{4.19}$$

where $\cos\theta_1'$ is defined in the q_1' rest frame (3.9) and β_1' is the boost factor in eq. (3.11a). In the $\beta_1' = 1$ limit, where the time-like vector-boson becomes on mass-shell and the two outgoing partons are emitted collinearly, we obtain

$$\cos\theta_1' = 2z_1' - \frac{1}{\beta_1'} \overset{\beta_1'=1}{\longrightarrow} 2z_1' - 1. \tag{4.20}$$

In the third column in tables 1(bottom) and 2(bottom), by making the replacement (4.20) in the $\beta_1' = 1$ limit, we present the splitting amplitudes for the outgoing fermion and gluon currents. There is no singularity for the $V^* \to f\bar{f}$ splitting amplitudes, while the $V^* \to gg$ amplitudes have the singularities at $z_1' = 0$ and 1, similar to the space-like gluon splitting amplitudes. This is because the singularities are associated only with soft gluon emissions.

Finally, let us confirm that the splitting amplitudes discussed above reproduce the standard (unregularized) quark and gluon splitting functions. From table 1(top), the sum

JHEP07(2009)101

of the squared amplitudes for the transversely-polarized vector-bosons ($\lambda_1 = \pm 1$), averaged/summed over initial/final parton helicities, leads to the $f \to V_T$ splitting function as

$$z_1 \frac{1}{2} \sum_{\sigma_{1,3}=\pm} \left[|\hat{\mathcal{J}}^{+}_{1\sigma_1\sigma_3}|^2 + |\hat{\mathcal{J}}^{-}_{1\sigma_1\sigma_3}|^2 \right] = \frac{1+(1-z_1)^2}{z_1} = P_{V_T/f}(z_1), \tag{4.21}$$

where the extra factor z_1 comes from the initial-state flux factor for the space-like branching. Similarly, from table 2(top) we can obtain the gluon splitting function as

$$z_1 \frac{1}{4} \sum_{\sigma_{1,3}=\pm} \left[|\hat{\mathcal{J}}^{+}_{1\sigma_1\sigma_3}|^2 + |\hat{\mathcal{J}}^{-}_{1\sigma_1\sigma_3}|^2 \right] = \frac{1-z_1}{z_1} + \frac{z_1}{1-z_1} + z_1(1-z_1) = P_{V_T/V_T}(z_1), \tag{4.22}$$

where, in addition to the spin averaged factor, we divide by the statistical factor for the two identical gluons in the final state. On the other hand, from the $V^* \to f\bar{f}$ splitting amplitudes in table 1(bottom), which are time-like branching, the $V_T \to f$ splitting function can be reproduced,

$$\frac{1}{2} \sum_{\sigma'_{1,3}=\pm} \left[|\hat{\mathcal{J}}'^{+}_{1\sigma'_1\sigma'_3}|^2 + |\hat{\mathcal{J}}'^{-}_{1\sigma'_1\sigma'_3}|^2 \right] = z_1'^{\,2} + (1-z_1'^{\,2}) = P_{f/V_T}(z'_1). \tag{4.23}$$

Likewise, from table 2(bottom), we can obtain the gluon splitting function as in eq. (4.22),

$$\frac{1}{4} \sum_{\sigma'_{1,3}=\pm} \left[|\hat{\mathcal{J}}'^{+}_{1\sigma'_1\sigma'_3}|^2 + |\hat{\mathcal{J}}'^{-}_{1\sigma'_1\sigma'_3}|^2 \right] = P_{V_T/V_T}(z'_1). \tag{4.24}$$

In the parton branching description, the space-like and time-like vector-bosons, i.e. gluons, are almost on mass-shell, and hence their polarization vectors are taken to be purely transverse. However, the longitudinal component of the polarization ($\lambda_1 = 0$) also exists for the massive vector-bosons. Therefore, in addition to the above standard parton splitting functions for the transversely-polarized vector-bosons, we list the functions for the longitudinal polarization:

$$z_1 \frac{1}{2} \sum_{\sigma_{1,3}=\pm} |\hat{\mathcal{J}}^{0}_{1\sigma_1\sigma_3}|^2 = \frac{2(1-z_1)}{z_1} = P_{V_L/f}(z_1) \qquad \text{from table 1(top)}, \tag{4.25}$$

$$z_1 \frac{1}{4} \sum_{\sigma_{1,3}=\pm} |\hat{\mathcal{J}}^{0}_{1\sigma_1\sigma_3}|^2 = \frac{(2-z_1)^2}{4z_1} = P_{V_L/V_T}(z_1) \qquad \text{from table 2(top)}, \tag{4.26}$$

$$\sum_{\sigma'_{1,3}=\pm} |\hat{\mathcal{J}}'^{0}_{1\sigma'_1\sigma'_3}|^2 = 4z'_1(1-z'_1) = P_{f/V_L}(z'_1) \qquad \text{from table 1(bottom)}, \tag{4.27}$$

$$\frac{1}{2} \sum_{\sigma'_{1,3}=\pm} |\hat{\mathcal{J}}'^{0}_{1\sigma'_1\sigma'_3}|^2 = \frac{1}{2}(2z'_1-1)^2 = P_{V_T/V_L}(z'_1) \qquad \text{from table 2(bottom)}. \tag{4.28}$$

In fact, many studies have been performed for Higgs boson productions via WBF in the equivalent weak-boson approximation, where the t-channel intermediate weak-bosons are viewed as partons in the incoming quarks and the above splitting functions $P_{V_L/f}$ as well as $P_{V_T/f}$ are considered [39]; see more details in ref. [34] and references therein.

JHEP07(2009)101

X	(λ)	V_i	$\Gamma^{\mu_1\mu_2}_{XV_1V_2}(q_1,q_2;\lambda)/g_{XV_1V_2}(q_1,q_2)$
H	(0)	W,Z	$g^{\mu_1\mu_2}$
H	(0)	$\gamma,Z/\gamma,g$	$q_1\cdot q_2\, g^{\mu_1\mu_2} - q_2^{\mu_1} q_1^{\mu_2}$
A	(0)	$\gamma,Z/\gamma,g$	$\epsilon^{\mu_1\mu_2\alpha\beta} q_{1\alpha} q_{2\beta}$
G	$(\pm2,\pm1,0)$	W,Z,γ,g	$\epsilon_{\alpha\beta}(P,\lambda)\,\hat{\Gamma}^{\alpha\beta,\mu_1\mu_2}_{GVV}(q_1,q_2)$

Table 3. The XVV vertex $\Gamma^{\mu_1\mu_2}_{XV_1V_2}(q_1,q_2;\lambda)$ in eq. (2.3), normalized by the scalar form factor $g_{XV_1V_2}(q_1,q_2)$, are defined for CP-even and -odd Higgs bosons (H and A) and massive gravitons (G), respectively. For the polarization tensor $\epsilon^{\alpha\beta}(P,\lambda)$ and the GVV vertex $\hat{\Gamma}^{\alpha\beta,\mu_1\mu_2}_{GVV}(q_1,q_2)$, see appendix A.

4.3 Off-shell VBF amplitudes

We will now show the final piece, the $VV \to X$ production and the $X \to VV$ decay amplitudes in eqs. (2.9) and (2.14), respectively. In this paper, we consider the productions and the decays of massive spin-0 and spin-2 bosons: neutral CP-even and CP-odd Higgs bosons ($X = H$ and A), and graviton resonances ($X = G$).

For the fusion vertex of a CP-even Higgs boson, we consider both the WBF process and the GF process through a top-quark loop in the SM, and their tensor structures $\Gamma^{\mu_1\mu_2}_{XV_1V_2}(q_1,q_2)$, normalized by the coupling form factors $g_{XV_1V_2}(q_1,q_2)$, are given in table 3. The constant coupling, $g_{HVV} = 2m_V^2/v$ ($V = W,Z$) with $v = 246\,\text{GeV}$, gives the WBF vertex, while the explicit expression of the form factor $g_{Hgg}(q_1,q_2)$ by a triangle-loop is given in ref. [2].[3] Note that in refs. [1, 3, 8, 10] the same loop-induced vertex structure has been considered to study the anomalous couplings between the Higgs and weak bosons. We also consider the GF vertex for a CP-odd Higgs boson, defined in table 3. For light Higgs bosons ($M_{H,A} < 2m_t$), the above Hgg and Agg vertices can be well described by the heavy-top effective Lagrangian [40–43]

$$\mathcal{L}_{H,A} = -\frac{1}{4} g_{Hgg} H F^a_{\mu\nu} F^{a,\mu\nu} + \frac{1}{2} g_{Agg} A F^a_{\mu\nu} \tilde{F}^{a,\mu\nu}, \tag{4.29}$$

where $F^{a,\mu\nu}$ is the gluon field-strength tensor and $\tilde{F}^{a,\mu\nu} = \frac{1}{2}\epsilon^{\mu\nu\rho\sigma} F^a_{\rho\sigma}$ is its dual. The coupling constants are given by $g_{Hgg} = \alpha_s g_{Htt}/3\pi m_t$ and $g_{Agg} = \alpha_s g_{Att}/2\pi m_t$. The same tensor structures can be written for the interactions of the CP-even/odd Higgs boson with two photons [44] and with a Z-boson and a photon [45].

For graviton resonances, we adopt the simplest RS model [16, 17], where only gravitons can propagate into the extra dimension, and consider the first excited mode of the Kaluza-Klein (KK) gravitons. The low-energy effective interactions with the SM fields are given by

$$\mathcal{L}_G = -\frac{1}{\Lambda} T^{\mu\nu} G_{\mu\nu}, \tag{4.30}$$

where $T^{\mu\nu}$ is the energy-momentum tensor of the SM fields (see, e.g., ref. [46] for the explicit forms) and $G_{\mu\nu}$ is the spin-2 KK graviton. The RS graviton excitations have the

[3] Strictly speaking, the Hgg coupling tensor is given by two terms as $T^{\mu_1\mu_2} = F_T T_T^{\mu_1\mu_2} + F_L T_L^{\mu_1\mu_2}$ [2], where $T_T^{\mu_1\mu_2}$ is identical with the form in table 3. However, we neglect the second term since it does not contribute in the on-shell gluon limit and is not enhanced in the collinear limit.

JHEP07(2009)101

		CP-even		CP-odd
λ	$(\lambda_1\lambda_2)$	H(WBF)	H(loop-induced)	A
0	$(\pm\pm)$	-1	$-\frac{1}{2}(M^2+Q_1^2+Q_2^2)$	$\mp\frac{i}{2}\sqrt{(M^2+Q_1^2+Q_2^2)^2-4Q_1^2Q_2^2}$
0	(00)	$\frac{M^2+Q_1^2+Q_2^2}{2Q_1Q_2}$	Q_1Q_2	0

Table 4. The reduced helicity amplitudes for the CP-even/odd Higgs boson productions via off-shell vector-boson fusion, $\hat{\mathcal{M}}_{X\,\lambda_1\lambda_2}^{\lambda}(V_{\lambda_1}^*V_{\lambda_2}^* \to H/A_\lambda)$, in the VBF frame. M is the Higgs boson mass, and Q_1 and Q_2 are magnitudes of the four-momentum squared of the vector bosons.

universal coupling strength of $1/\Lambda$ to the matter and gauge fields, e.g. $g_{GVV} = -1/\Lambda$ ($V = W, Z, \gamma, g$), where Λ is the scale parameter of the theory and can be a few TeV. The explicit forms of the polarization tensor for a spin-2 graviton and the three-point GVV vertices are given in appendix A.

In table 4, we present the reduced helicity amplitudes for the CP-even/odd Higgs boson productions via off-shell vector-bosons, $\hat{\mathcal{M}}_{X\,\lambda_1\lambda_2}^{\lambda}(V_{\lambda_1}^*V_{\lambda_2}^* \to H/A_\lambda)$, where

$$\begin{aligned}\left(\mathcal{M}_{V_1V_2}^{X}\right)_{\lambda_1\lambda_2}^{\lambda} &= \epsilon_{\mu_1}(q_1,\lambda_1)\,\epsilon_{\mu_2}(q_2,\lambda_2)\,\Gamma_{XV_1V_2}^{\mu_1\mu_2}(q_1,q_2;\lambda)^* \\ &= g_{XV_1V_2}(q_1,q_2)\,\hat{\mathcal{M}}_{X\,\lambda_1\lambda_2}^{\lambda},\end{aligned} \tag{4.31}$$

in the VBF frame. Since Higgs bosons are spin-0 particles ($\lambda = 0$), we have the helicity selection rule ($\lambda_1 = \lambda_2$), and hence only three amplitudes among the nine amplitudes which have the different helicity combinations of the colliding vector-bosons can be nonzero. In the table, the amplitudes are expressed in terms of the Higgs boson mass M and magnitudes of the four-momentum squared of the vector bosons Q_1 and Q_2. The amplitudes for the CP-even and CP-odd Higgs bosons via the collisions of the transversely-polarized vector-bosons have the relationships, respectively,

$$\hat{\mathcal{M}}_{H++} - \hat{\mathcal{M}}_{H--} = 0, \tag{4.32}$$

$$\hat{\mathcal{M}}_{A++} + \hat{\mathcal{M}}_{A--} = 0. \tag{4.33}$$

Moreover, the pseudoscalar Higgs bosons (A) cannot be produced through the longitudinal vector-bosons, $\hat{\mathcal{M}}_{A00} = 0$, due to the CP-odd property. We should notice that, in the case of $Q_1, Q_2 \ll M$, the Higgs bosons via WBF are produced mostly through the longitudinally-polarized weak-bosons. On the other hand, the loop-induced CP-even (CP-odd) Higgs bosons are produced mainly (only) by the transversely-polarized vector-bosons, and the magnitude of their amplitudes are almost equal, $|\hat{\mathcal{M}}_H| \sim |\hat{\mathcal{M}}_A|$, apart from the overall coupling factors. These characters of the XVV amplitudes, together with the phases of the current amplitudes, play an important role to develop the distinctive azimuthal angle correlations of the jets.

Similarly, table 5 shows the reduced helicity amplitudes for the massive-graviton productions via off-shell vector-bosons, $\hat{\mathcal{M}}_{X\,\lambda_1\lambda_2}^{\lambda}(V_{\lambda_1}^*V_{\lambda_2}^* \to G_\lambda)$, in the VBF frame, where $\lambda = \lambda_1 - \lambda_2$ is the tensor helicity along the colliding vector-boson axis (positive z-axis).

JHEP07(2009)101

λ	$(\lambda_1\lambda_2)$	G
±2	$(\pm\mp)$	$-(M^2+Q_1^2+Q_2^2+2m_V^2)$
±1	(±0)	$\frac{1}{\sqrt{2}MQ_2}\left[Q_2^2(M^2-Q_1^2+Q_2^2)-m_V^2(M^2+Q_1^2-Q_2^2)\right]$
±1	$(0\mp)$	$\frac{1}{\sqrt{2}MQ_1}\left[Q_1^2(M^2+Q_1^2-Q_2^2)-m_V^2(M^2-Q_1^2+Q_2^2)\right]$
0	$(\pm\pm)$	$\frac{1}{\sqrt{6}M^2}\left[(Q_1^2-Q_2^2)^2+M^2(Q_1^2+Q_2^2-2m_V^2)\right]$
0	(00)	$-\frac{1}{\sqrt{6}Q_1Q_2}\Big[4Q_1^2Q_2^2+2m_V^2(M^2+Q_1^2+Q_2^2)$ $-\frac{m_V^2}{M^2}\{(M^2+Q_1^2+Q_2^2)^2-4Q_1^2Q_2^2\}\Big]$

Table 5. The same as table 4, but for the massive-graviton productions, $V^*_{\lambda_1}V^*_{\lambda_2}\to G_\lambda$, where M and m_V is the graviton and the vector-boson mass, respectively.

For the spin-2 particle productions, the amplitudes in all the helicity combinations of the vector bosons exist, that is, the nine amplitudes are registered in table 5. However, in the case of $Q_1, Q_2 \ll M$, the $\lambda=\pm2$ states of the gravitons are dominantly produced for the massless vector-boson collisions, when the vector bosons have the opposite-sign transverse polarizations. For the massive vector-boson case, on the other hand, the amplitudes of other three states ($\lambda=\pm1$ and 0) are not negligible.

The $X\to VV$ decay helicity amplitudes in eq. (2.14), $\left(\mathcal{M}'^{X}_{V_1'V_2'}\right)^{\lambda'}_{\lambda_1'\lambda_2'}$, are obtained from the above $VV\to X$ fusion amplitudes (tables 4 and 5) by making the replacements $Q_i^2\to -Q_i'^2$, where λ_1' and λ_2' are the helicities of the decaying vector-bosons and $\lambda'=\lambda_1'-\lambda_2'$ is the X helicity along the momentum direction of the vector bosons (z'-axis in figure 3). We note that for the non-scalar particle decays the dependence of the angle Θ between the initial polarization λ along the z-axis and the final polarization λ' along the z'-axis is dictated by a d function and factorized in our convention; see eq. (2.16).

At this point it is worth noting that the amplitudes of the Higgs boson decays into transversely-polarized weak-bosons ($\hat{\mathcal{M}}'_{H\pm\pm}$) are comparable to that into longitudinal ones ($\hat{\mathcal{M}}'_{H00}$) near the VV threshold, while the longitudinal amplitudes are dominant for large Higgs boson masses. This is because one or both of the weak bosons can become on-shell and the typical mass scale of the decaying weak-bosons are $Q_i\sim m_V$. The helicity amplitudes of the Higgs boson decays into the on-shell weak-bosons are given by

$$\hat{\mathcal{M}}'_{H\pm\pm}=-1,\quad \hat{\mathcal{M}}'_{H00}=\frac{M^2}{2m_V^2}-1=\gamma'^2(1+\beta'^2), \tag{4.34}$$

where $\beta'=\sqrt{1-4m_V^2/M^2}$ and $\gamma'=1/\sqrt{1-\beta'^2}$ are the velocity and the Lorentz-boost factor of the weak bosons, respectively.[4]

It may be also useful to present the helicity amplitudes for the graviton decays into a on-shell vector-boson pair; see table 6, which can be reduced from the $VV\to G$ amplitudes

[4]See ref. [32] for the amplitudes of the Higgs boson decays into a pair of virtual and real weak-bosons with the most general HV^*V vertices.

JHEP07(2009)101

λ'	$(\lambda'_1\lambda'_2)$	G
± 2	$(\pm\mp)$	$-M^2$
± 1	$(\pm 0), (0\mp)$	$\frac{1}{\sqrt{2}}\sqrt{1-\beta'^2}\,M^2$
0	$(\pm\pm)/(00)$	$-\frac{1}{\sqrt{6}}(1-\beta'^2)\,M^2 \,/\, -\frac{1}{\sqrt{6}}(2-\beta'^2)\,M^2$

Table 6. The reduced helicity amplitudes for the massive-graviton decays into a on-shell vector-boson pair, $\hat{\mathcal{M}}'_{X\,\lambda'_1\lambda'_2}(G_{\lambda'} \to V_{\lambda'_1} V_{\lambda'_2})$, in the graviton rest frame.

in table 5 with the replacements $Q_i^2 \to -m_V^2$. In the heavy graviton-mass limit, or in the $\beta' = 1$ limit, only three (two) amplitudes among the nine survive for the decays into massive (massless) vector-bosons.

5 Azimuthal angle correlations

We are now ready to present the helicity amplitudes explicitly for the X productions with 2 jets via VBF, eq. (2.7), and the X decays into 4 jets via a vector-boson pair, eq. (2.15). In this section, we demonstrate that the VBF amplitudes dominate the exact matrix elements by appropriate selection cuts to the final state [47], and then show that nontrivial azimuthal angle correlations of the jets in the production are manifestly expressed as the quantum interference among different helicity states of the intermediate vector-bosons. We also discuss the X decay angular correlations.

5.1 The VBF amplitudes vs. the full amplitudes

Although we have considered only the VBF diagrams in figure 1, there are other crossing-related diagrams which have to be taken into account. Representative Feynman diagrams for each subprocess, including the VBF diagrams, are shown in figure 4.

The Higgs bosons are emitted from each of the circle points in the diagrams. (a) $qq \to qqH/A$: The Higgs boson is radiated off the weak-boson propagator, or the gluon (photon) propagator through a top-quark triangle-loop. There is only a t-channel VBF diagram in the case of the different-flavor initial state, while an additional s-channel diagram or a u-channel diagram exists in the identical-flavor case. (b) $qg \to qgH/A$: In addition to the H/Agg coupling along the gluon lines, the process receives the $H/Aggg$ box-loop contribution on the gluon three-point vertex. There are in total 8 diagrams in the large-m_t limit,[5] in which the top-quark loop is replaced by the effective coupling. (c) $gg \to ggH/A$: Besides the three corresponding $gg \to gg$ processes in figure 4(c), the u-channel diagram exists. There are 26 diagrams in the heavy-top limit, including one diagram with the effective $Hgggg$ vertex induced via a pentagon loop.[6]

The KK gravitons are emitted from both the circle and the square points in the diagrams in figure 4, due to their universal couplings to the matter and gauge fields. There-

[5] Away from the heavy-top limit, the number of diagrams increases because of the ordering of the gluon momenta along the top-quark loop [2].

[6] A CP-odd Higgs boson does not have the $Agggg$ vertex due to the anti-symmetric nature of the coupling [43].

JHEP07(2009)101

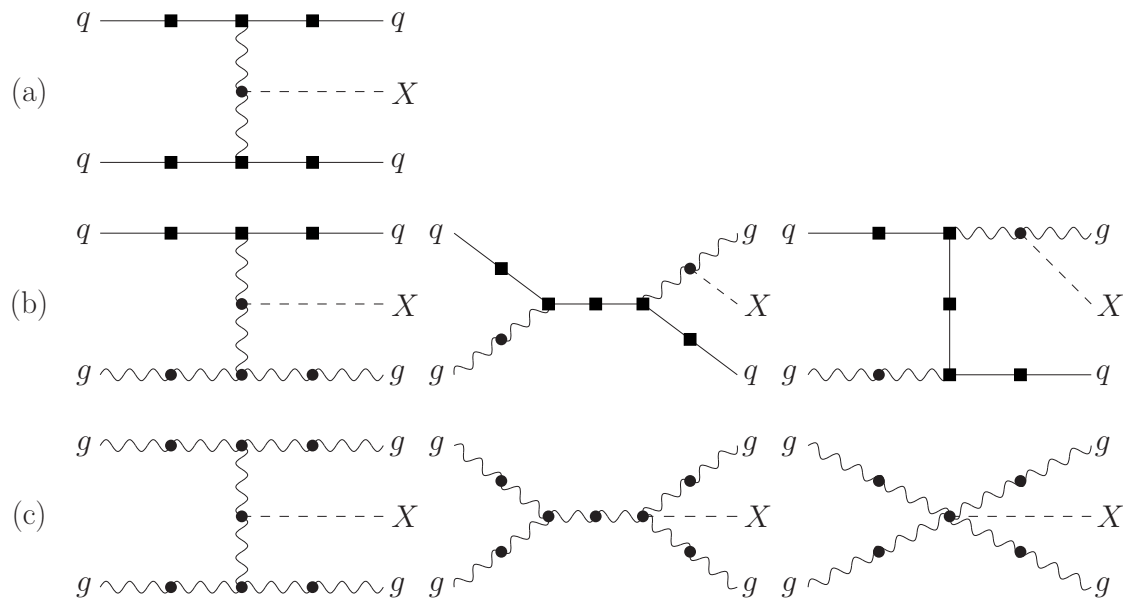

Figure 4. Representative Feynman diagrams for the subprocesses, (a) $qq \to qqX$, (b) $qg \to qgX$, (c) $gg \to ggX$, which contribute to the X + 2-jet production at hadron colliders, $pp \to jjX$. The Higgs bosons are emitted from each of the circle points in the diagrams, while the KK gravitons are emitted from each of the circle and square points.

fore, the graviton productions have many more diagrams even in quark-quark scatterings (figure 4(a)).

The point which must be investigated here is whether the VBF amplitudes can dominate the exact matrix elements, in which all the possible diagrams contribute. Our key observation is that this happens when we select those events which satisfy the characteristic kinematical structure of the VBF processes. Due to the t-channel propagators of the vector bosons in the VBF amplitudes in eq. (2.7), the Xjj events via VBF are dominantly produced when both $Q_1 \left(= \sqrt{-q_1^2} \right)$ and $Q_2 \left(= \sqrt{-q_2^2} \right)$ are small. In other words, the intermediate vector-bosons in the VBF processes tend to carry only a small fraction of the initial parton energies. For small Q_1 and Q_2, the initial partons scatter to far forward and far backward, and the heavy particle X is produced centrally. Therefore, the two jets have the large rapidity gap, which is often used as the so-called WBF cut to enhance the WBF Higgs productions. It should be stressed that this kinematical feature is not particular to the WBF production processes, but the QCD productions via the t-channel GF processes in qq, qg and gg collisions also have the similar kinematical structure. This suggests that some kinematical cuts, such as a large rapidity separation between two jets, may select the VBF diagrams dominantly among all the possible diagrams.

Let us demonstrate numerically that the dijet large rapidity separation is an effective kinematical cut to select the VBF amplitudes among the full amplitudes. As the minimal selection cuts on the final-state partons, we impose the following kinematical constraints

JHEP07(2009)101

$\sigma_{\rm VBF}/\sigma_{\rm exact}$	$\Delta\eta_{jj} > 3$	$\Delta\eta_{jj} > 4$	$\Delta\eta_{jj} > 5$
$qq \to qqH/A/G$	1.00/1.00/1.58	1.00/1.00/1.43	1.00/1.00/1.25
$qg \to qgH/A/G$	1.07/1.05/1.30	1.04/1.03/1.18	1.02/1.02/1.11
$gg \to ggH/A/G$	1.07/1.06/1.16	1.04/1.04/1.11	1.02/1.02/1.07

Table 7. Ratio of the VBF contribution to the cross section with the exact matrix elements, $\sigma_{\rm VBF}/\sigma_{\rm exact}$, for each subprocess at the LHC, after imposing the inclusive cuts (5.1) and the VBF cuts (5.2) with $\Delta\eta_{jj\rm min} = 3$, 4 and 5.

for the LHC, required by the detector and jet algorithms:

$$p_{T_j} > 20 \text{ GeV}, \quad |\eta_j| < 5, \quad R_{jj} = \sqrt{\Delta\eta_{jj}^2 + \Delta\phi_{jj}^2} > 0.6, \tag{5.1}$$

where p_{T_j} and η_j are the transverse momentum and the pseudorapidity of a final-state parton, respectively, and R_{jj} describes the separation of the two partons in the plane of the pseudorapidity and the azimuthal angle. Moreover, in order to select the VBF contributions, the two tagging jets are required to reside in opposite detector hemispheres and to be well separated in rapidity,

$$\eta_{j_1} > 0 > \eta_{j_2}, \quad \Delta\eta_{jj} = \eta_{j_1} - \eta_{j_2} > \Delta\eta_{jj\rm min}. \tag{5.2}$$

Varying the value of $\Delta\eta_{jj\rm min}$, we study the fraction of the VBF contributions to the cross section with the exact matrix elements. The analyses are done at the parton level with tree-level matrix elements. The exact matrix elements for the Higgs boson productions are calculated by `HELAS` subroutines [38], generated by the `HEFT` (Higgs effective field theory) model in `MadGraph/MadEvent` (`MG/ME`) `v4` [48]. For the massive-graviton productions, the relevant `HELAS` subroutines for massive spin-2 particles and its interactions based on the effective Lagrangian of eq. (4.30) have also been implemented into `MG/ME` [46]. Numerical integrations are done with the help of the Monte Carlo integration program `BASES` [49]. Throughout our numerical study, we employ the CTEQ6L1 parton distribution functions [50] with the factorization scale chosen as the geometric mean of the jet transverse momenta $\mu_f = \sqrt{p_{T_{j_1}} p_{T_{j_2}}}$, and fix the QCD coupling at $\alpha_s = \alpha_s^{\rm LO}(m_Z) = 0.13$. Unless specified, we set the heavy particle mass at $M = 600\,\text{GeV}$ and the scale of the RS model at $\Lambda = 4\,\text{TeV}$, which corresponds to the current lower bound for the mass of the first KK mode of massive gravitons [17, 24]. Note that we use the constant value for the Higgs effective couplings in spite of $M_{H,A} > 2m_t$, because the energy dependence of the effective couplings are almost canceled out when the ratio of the cross sections is considered, and because the azimuthal angle distributions are insensitive to the form factor effects [8].

In table 7, we show the ratio of the VBF contribution ($\sigma_{\rm VBF}$) to the cross section with the exact matrix elements ($\sigma_{\rm exact}$) for the nine subprocesses at the LHC, after imposing the inclusive cuts (5.1) and the VBF selection cuts (5.2) with $\Delta\eta_{jj\rm min} = 3$, 4 and 5. For all the subprocesses, as the rapidity separation increases, the VBF contributions tend to dominate the exact matrix elements and the ratios approach unity. In the first row, the CP-even and -odd Higgs production processes in qq collisions, where we consider ud collisions for

JHEP07(2009)101

$\sigma_{\rm VBF}/\sigma_{\rm exact}$	$\Delta\eta_{jj} > 3$	$\Delta\eta_{jj} > 4$	$\Delta\eta_{jj} > 5$
$qq \to qqH/A/G$	1.00/1.00/1.02	1.00/1.00/1.02	1.00/1.00/1.02
$qg \to qgH/A/G$	1.04/1.04/1.07	1.03/1.03/1.06	1.02/1.02/1.04
$gg \to ggH/A/G$	1.05/1.05/1.09	1.04/1.04/1.07	1.02/1.02/1.05

Table 8. The same as table 7, but imposing the additional p_{T_j} cut of eq. (5.3).

simplicity, have only the VBF diagrams, and hence $\sigma_{\rm VBF}/\sigma_{\rm exact} = 1$.[7] Although the cross sections in qg and gg collisions have non-VBF diagrams, their contributions are rather small after the VBF cuts. On the other hand, for the massive-graviton production, the gravitons are emitted also from the quark lines, as shown in figures 4 (a) and (b), and the ratio deviates significantly from unity especially in qq collisions. Furthermore, their contributions do not diminish swiftly when the rapidity separation cut is increased from 3 to 5. We note here that the electroweak contributions to the $qq \to qqG$ process represent a small correction, which is below 1%, even when the VBF cuts are imposed [27].

In case of the massive-graviton production, the non-VBF contributions are significant even after the VBF selection cuts with $\Delta\eta_{jj\rm min} = 5$. We therefore examine the impact of an additional cut on the transverse momenta of the tagging jets,

$$p_{T_j} < 100 \text{ GeV}. \tag{5.3}$$

table 8 shows the same ratio of the VBF contribution to the exact cross section when this additional cut is imposed. We find that the above p_{T_j} cut works effectively to suppress contributions from the non-VBF diagrams, especially the diagrams which emit the graviton from the quark lines. This is because the quarks that emit a graviton tends to have high transverse momenta.

Summing up, from table 7, the large rapidity separation may guarantee the validity of our VBF analyses not only for the WBF Higgs productions but also for the GF processes. Moreover, from table 8, the p_{T_j} slicing cut,

$$20 \text{ GeV} < p_{T_j} < 100 \text{ GeV}, \tag{5.4}$$

from eqs. (5.1) and (5.3) is effective in selecting the GF contribution to the graviton production processes. It should be noticed that stringent cuts increase the VBF contributions but reduce the primary event number.

As a reference, we present the total cross sections with the exact matrix elements for the massive-graviton productions in table 9, where the inclusive cuts (5.1) and the VBF cuts (5.2) without and with the p_{T_j} slicing cut (5.4) are imposed. For the cross section of the Higgs boson productions, see figure 4 in ref. [2]. In the following analyses, we take $\Delta\eta_{jj\rm min} = 4$ in the VBF cuts (5.2) for the Higgs and graviton productions, and further apply the p_{T_j} slicing cut (5.4) for the graviton productions.

[7] Even for the collisions of identical-flavor quarks, the s- or u-channel contribution is negligible when the VBF cuts are applied [11]. In addition, the interferences between the electroweak and QCD contributions are very small [12, 51, 52].

JHEP07(2009)101

	$20\ \text{GeV} < p_{T_j}$			$20\ \text{GeV} < p_{T_j} < 100\ \text{GeV}$		
σ_{exact} [pb]	$\Delta\eta_{jj} > 3$	$\Delta\eta_{jj} > 4$	$\Delta\eta_{jj} > 5$	$\Delta\eta_{jj} > 3$	$\Delta\eta_{jj} > 4$	$\Delta\eta_{jj} > 5$
$qq \to qqG$	2.0	1.6	1.1	0.7	0.6	0.5
$qg \to qgG$	13.2	8.8	4.7	7.2	5.5	3.3
$gg \to ggG$	15.9	8.0	3.2	11.7	6.2	2.7

Table 9. The total cross sections with the exact matrix elements for each subprocess of the massive-graviton plus dijet events at the LHC, after imposing the inclusive cuts (5.1) and the VBF cuts (5.2) without and with the additional p_{T_j} cut of eq. (5.3), for $M_G = 600\,\text{GeV}$ and $\Lambda = 4\,\text{TeV}$.

5.2 Correlations in the production with two associated jets

We are now able to discuss the angular correlations of the two accompanying jets in the X productions, using our analytical VBF amplitudes.

The production and decay density matrices in eq. (2.17) have all information on the angular correlations between the jets in the productions and the decays of the heavy particle X. In this section, we consider the $n = 2$ case in (2.17) to investigate the angular correlation between the two jets in the Xjj productions, while, to simplify the decay part, we consider the $n' = 2$ case and fix the X polarization along the 2-body decay axis (z'-axis), $\lambda' = \sigma'_1 - \sigma'_2 = \pm 2$, ± 1, or 0. We note that, in practice, we can project out σ'_1 and σ'_2 by properly weighting the final states of a'_1 and a'_2 decays in the $X \to a'_1 a'_2$ decays; e.g. for the $X \to W^+W^-$ decays we can project out all the five cases, $\lambda' = \pm 2$, ± 1, and 0, while the $X \to \gamma\gamma$ or gg decays give only the sum of $\lambda' = +2$ and -2. Moreover, the $X \to \tau^+\tau^-$ decay process can project out $\lambda' = +1$ and -1 cases, while for the e or μ case we cannot distinguish these two. In the following we take $\lambda' = \bar{\lambda}'$ and suppress the decay density matrix in eq. (2.17).

For the VBF processes (2.1), the production density matrix is given in eq. (2.19a) in terms of the production tensor $\mathcal{P}^{\lambda_1\lambda_2}_{\bar{\lambda}_1\bar{\lambda}_2}$ of eq. (2.20a). The tensor has 81 independent jet angular distributions in terms of the polar ($\theta_{1,2}$) and azimuthal ($\phi_{1,2}$) angles of the two tagging jets. When we isolate the azimuthal angle dependence in eq. (2.17), there are 25 distributions (including one constant piece) as

$$\begin{aligned}\mathcal{P}^{\lambda_1\lambda_2}_{\bar{\lambda}_1\bar{\lambda}_2} d^J_{\lambda,\lambda'} d^J_{\bar{\lambda},\lambda'} = F_1 + \big\{2\,\Re e\big[&F_2\cos\phi_1 + F_3\cos\phi_2 + F_4\cos 2\phi_1 + F_5\cos 2\phi_2 \\ &+ F_6^{\pm}\cos(\phi_1 \pm \phi_2) + F_7^{\pm}\cos(2\phi_1 \pm \phi_2) + F_8^{\pm}\cos(\phi_1 \pm 2\phi_2) \\ &+ F_9^{\pm}\cos 2(\phi_1 \pm \phi_2)\big] + (\Re e \to \Im m,\ \cos \to \sin)\big\}. \end{aligned} \tag{5.5}$$

Here, and in the following, summation over repeated indices $(\lambda_1, \lambda_2, \bar{\lambda}_1, \bar{\lambda}_2) = \pm, 0$ is implied, and a shorthand notation such as $F_6^{\pm}\cos(\phi_1 \pm \phi_2)$ for $F_6^{+}\cos(\phi_1+\phi_2) + F_6^{-}\cos(\phi_1-\phi_2)$ is used. The coefficients $F_i^{(\pm)}$ are the functions of the kinematical variables except the azimuthal angles $\phi_{1,2}$. For the productions of spin-full heavy particles, they also depend on the decay angle Θ which comes from the product of two d functions. For the spin-0 particle case, only the five terms in eq. (5.5) survive due to the helicity selection $\lambda_1 = \lambda_2$, which will be discussed in the next subsection 5.2.1. All the *sine* terms vanish when CP is conserved and when the absorptive part of the amplitudes are neglected, e.g., in the

JHEP07(2009)101

tree-level approximation. It should be noted that the azimuthal angle variables, ϕ_1 and ϕ_2, are individually defined in the VBF frame by the scattering plane of the subprocess, $V_1^* V_2^* \to X \to a_1' a_2'$; see also figure 3.

Because the phases of the quark and gluon current amplitudes are the same for each helicity combination (see tables 1(top) and 2(top)), and because the phase of the product of the two currents for $\sigma_1 = \sigma_3$ and $\sigma_2 = \sigma_4$ is (see eq. (4.6))

$$\hat{\mathcal{J}}_{1\,\sigma_1,\sigma_3=\sigma_1}^{\lambda_1} \hat{\mathcal{J}}_{2\,\sigma_2,\sigma_4=\sigma_2}^{\lambda_2} \propto e^{-i(\lambda_1\phi_1 - \lambda_2\phi_2)}, \tag{5.6}$$

the coefficients $F_{1-9}^{(\pm)}$ for qq, qg and gg collisions are expressed in terms of the production tensors $\mathcal{P}_{\lambda_1\lambda_2}^{\lambda_1\lambda_2}$ and two d functions as

$$\begin{aligned}
F_1 &= \mathcal{P}_{\lambda_1\lambda_2}^{\lambda_1\lambda_2} d^J_{\lambda_1-\lambda_2,\lambda'} d^J_{\lambda_1-\lambda_2,\lambda'},\\
F_2 &= \mathcal{P}_{0\lambda_2}^{+\lambda_2} d^J_{1-\lambda_2,\lambda'} d^J_{-\lambda_2,\lambda'} + \mathcal{P}_{-\lambda_2}^{0\lambda_2} d^J_{-\lambda_2,\lambda'} d^J_{-1-\lambda_2,\lambda'},\\
F_3 &= \mathcal{P}_{\lambda_1+}^{\lambda_1 0} d^J_{\lambda_1,\lambda'} d^J_{\lambda_1-1,\lambda'} + \mathcal{P}_{\lambda_1 0}^{\lambda_1-} d^J_{\lambda_1+1,\lambda'} d^J_{\lambda_1,\lambda'},\\
F_4 &= \mathcal{P}_{-\lambda_2}^{+\lambda_2} d^J_{1-\lambda_2,\lambda'} d^J_{-1-\lambda_2,\lambda'},\\
F_5 &= \mathcal{P}_{\lambda_1+}^{\lambda_1-} d^J_{\lambda_1+1,\lambda'} d^J_{\lambda_1-1,\lambda'},\\
F_6^{\pm} &= \mathcal{P}_{0\pm}^{+0} d^J_{1,\lambda'} d^J_{-1/1,\lambda'} + \mathcal{P}_{00}^{+\mp} d^J_{2/0,\lambda'} d^J_{0,\lambda'} + \mathcal{P}_{-\pm}^{00} d^J_{0,\lambda'} d^J_{-2/0,\lambda'} + \mathcal{P}_{-0}^{0\mp} d^J_{1/-1,\lambda'} d^J_{-1,\lambda'},\\
F_7^{\pm} &= \mathcal{P}_{-\pm}^{+0} d^J_{1,\lambda'} d^J_{-2/0,\lambda'} + \mathcal{P}_{-0}^{+\mp} d^J_{2/0,\lambda'} d^J_{-1,\lambda'},\\
F_8^{\pm} &= \mathcal{P}_{0\pm}^{+\mp} d^J_{2/0,\lambda'} d^J_{-1/1,\lambda'} + \mathcal{P}_{-\pm}^{0\mp} d^J_{1/-1,\lambda'} d^J_{-2/0,\lambda'},\\
F_9^{\pm} &= \mathcal{P}_{-\pm}^{+\mp} d^J_{2/0,\lambda'} d^J_{-2/0,\lambda'}.
\end{aligned} \tag{5.7}$$

This relations can be also applied to the processes with the helicity-flip currents, namely the cases for $\sigma_1 = -\sigma_3$ and/or $\sigma_2 = -\sigma_4$, which appear only in the gluon currents, although they have the different phase from those with the conserved currents in eq. (5.6). The process that one of the currents is helicity-flip (the case in $\sigma_1 = -\sigma_3$ or $\sigma_2 = -\sigma_4$) leads nontrivial azimuthal distributions from F_2 through F_5, while the case that the both currents are helicity-flip gives rise to only the constant piece, F_1. This is because the helicity-flip gluon splitting amplitudes emit an off-shell gluon of definite helicity; see table 2. On the other hand, the helicity-conserved processes ($\sigma_1 = \sigma_3$ and $\sigma_2 = \sigma_4$) can contribute to all the terms, as can be seen from table 1 for the quark currents and table 2 for the gluon currents. We note that the magnitude of the correlations is determined by the relative ratio to the constant term F_1.

It should be stressed here that in eq. (5.7) the Θ-dependent azimuthal angle correlations are manifestly expressed by quantum interference among different helicity states of the intermediate vector-bosons. We also notice that the above formulae can be applied to any spin-J particle productions through the VBF processes, although massive spin-0 and -2 particles are considered in this article.

5.2.1 Higgs boson productions

For the scalar particle productions, only the three off-shell VBF amplitudes, $\hat{\mathcal{M}}_{X++}$, $\hat{\mathcal{M}}_{X00}$ and $\hat{\mathcal{M}}_{X--}$, in which the colliding vector-bosons have the same helicities ($\lambda_1 = \lambda_2$),

JHEP07(2009)101

can contribute to the production amplitude (2.7), and there is no Θ dependence, namely $d^{J=0}_{\lambda,\lambda'}(\Theta) = 1$ in eq. (5.5) (and in eq. (5.7)). Therefore, the azimuthal angle correlation (5.5) is reduced to

$$\mathcal{P}^{\lambda_1\lambda_2}_{\bar\lambda_1\bar\lambda_2} = F_1 + \left\{2\,\Re e\left[F_6^- \cos\Delta\phi_{12} + F_9^- \cos 2\Delta\phi_{12}\right] + (\Re e \to \Im m,\ \cos \to \sin)\right\} \tag{5.8}$$

with $\Delta\phi_{12} \equiv \phi_1 - \phi_2$, which is the azimuthal angle separation of the two tagging jets. As mentioned above, the azimuthal dependence is manifestly expressed by the quantum interference terms among different helicity states of the intermediate vector-bosons; the F_6^- $(= \mathcal{P}^{++}_{00} + \mathcal{P}^{00}_{--})$ term is induced through the interference between the production with the longitudinal and transverse polarization states of the vector bosons, while the F_9^- $(= \mathcal{P}^{++}_{--})$ term is caused by the interference between the two transverse polarization states.

Now we can observe clearly the origin of the nontrivial azimuthal angle correlations for the CP-even and CP-odd Higgs bosons (H and A), predicted in refs. [1–4]. As we mentioned in section 4.3, in the case of $Q_1, Q_2 \ll M$, where the VBF contributions are dominant, the Higgs bosons with a $g^{\mu\nu}$-type coupling are produced mostly through the longitudinally-polarized vector-bosons. Therefore, the $\hat{\mathcal{M}}_{H00}$ amplitude dominates the total amplitudes, and hence there is little interference terms in eq. (5.8). This is why the WBF processes give the flat azimuthal angle correlation,

$$d\hat\sigma_{H(\mathrm{WBF})} \sim F_1. \tag{5.9}$$

For the loop-induced GF Higgs boson couplings, on the other hand, they are mainly produced by the transversely-polarized vector-bosons, namely the $\hat{\mathcal{M}}_{H/A++}$ and $\hat{\mathcal{M}}_{H/A--}$ amplitudes have the dominant contribution. Therefore, by the relations in (4.32) and (4.33), the azimuthal distributions are

$$d\hat\sigma_{H/A(\mathrm{GF})} \sim \left[F_1 \pm 2\,|F_9^-|\cos 2\Delta\phi_{12}\right], \tag{5.10}$$

where the $+/-$ sign is for CP-even/odd Higgs bosons. One can clearly see that the azimuthal distribution is strongly suppressed (enhanced) around $\Delta\phi_{12} = \pi/2$ for the GF CP-even (-odd) Higgs boson productions. We note that the F_6^- term in eq. (5.8) is exactly zero not only for the CP-odd Higgs boson production but also for the GF CP-even Higgs boson production since it measures the P-odd amplitude.

From the relations in (5.7) and by using the explicit forms of the amplitudes in tables 1(top), 2(top) and 4, the coefficient functions F_1 and F_9^- in eq. (5.10) for each subprocess, qq, qg and gg scatterings, are given by

$$\hat F_1[qq] = (1+\cos^2\theta_1)(1+\cos^2\theta_2), \tag{5.11a}$$

$$\hat F_1[qg] = \frac{1}{\sin^2\theta_2}(1+\cos^2\theta_1)(1+3\cos^2\theta_2)^2 \quad \text{or} \quad (1 \leftrightarrow 2), \tag{5.11b}$$

$$\hat F_1[gg] = \frac{1}{\sin^2\theta_1\sin^2\theta_2}(1+3\cos^2\theta_1)^2(1+3\cos^2\theta_2)^2, \tag{5.11c}$$

and

$$\hat F_9^-[qq/qg/gg] = \pm\frac{1}{2}(1-\cos^2\theta_1)(1-\cos^2\theta_2). \tag{5.12}$$

JHEP07(2009)101

Here we take the $Q_1, Q_2 \ll M$ limit for the $VV \to X$ amplitudes, where the only surviving amplitudes are $|\hat{\mathcal{M}}_{H/A\pm\pm}| = \frac{1}{2}M^2$ (see table 4), with the common overall factor

$$F_i^{(\pm)} = \frac{g_s^4 g_{H/Agg}^2 M^4 Q_1^2 Q_2^2}{2\cos^2\theta_1 \cos^2\theta_2}\, \hat{F}_i^{(\pm)}. \tag{5.13}$$

Note that we suppress the color factors, which are relevant to the ratio of the qq, qg and gg contributions in realistic simulations. It is remarkable that the interference term F_9^-, which receives the contribution only from the helicity-conserved amplitudes ($\sigma_1 = \sigma_3$ and $\sigma_2 = \sigma_4$), is same for all qq, qg and gg collision processes. Meanwhile F_1 has the different contributions from the quark currents and the gluon currents, which includes the helicity-flip contributions ($\sigma_1 = -\sigma_3$ and/or $\sigma_2 = -\sigma_4$), and can be larger as the process involves the gluon currents. These indicate that the gluon currents reduce the interference effect. It may be worth presenting the above functions in terms of the $z_{1,2}$ variables in the collinear limit ($\beta_{1,2} \to 1$) in eq. (4.18):

$$\hat{F}_1[qq] = 4(2 - 2z_1 + z_1^2)(2 - 2z_2 + z_2^2), \tag{5.14a}$$

$$\hat{F}_1[qg] = \frac{8}{(1 - z_2)}(2 - 2z_1 + z_1^2)(1 - z_2 + z_2^2)^2 \quad \text{or} \quad (1 \leftrightarrow 2), \tag{5.14b}$$

$$\hat{F}_1[gg] = \frac{16}{(1 - z_1)(1 - z_2)}(1 - z_1 + z_1^2)^2(1 - z_2 + z_2^2)^2, \tag{5.14c}$$

and

$$\hat{F}_9^-[qq/qg/gg] = \pm 8(1 - z_1)(1 - z_2), \tag{5.15}$$

with

$$F_i^{(\pm)} = \frac{g_s^4 g_{H/Agg}^2 M^4 Q_1^2 Q_2^2}{2 z_1^2 z_2^2}\, \hat{F}_i^{(\pm)}. \tag{5.16}$$

To examine the validity of the above analytic parton-level expectations, we plot in figure 5 the normalized azimuthal correlations $\Delta\phi_{12}$ (mod 2π) between the two tagging jets in the Higgs + 2-jet productions at the LHC, where the selection cuts (5.1) and (5.2) with $\Delta\eta_{jj\min} = 4$ are applied. The distributions for each subprocess with the full diagrams and those with the VBF diagrams only are shown by solid and dashed lines, respectively. The VBF contributions can reproduce the distributions with the exact matrix elements very well not only for the WBF processes but also for the GF processes. As mentioned in the introduction, these azimuthal angle correlations predicted in the leading order may survive even after higher-order corrections are applied [13, 15].

It may be worth pointing out here that, even though our definition of the azimuthal angles of the jets, which are measured along the vector-boson colliding axis, is different from the usual definition along the beam axis in the laboratory frame, the $\Delta\phi_{12}$ distributions are almost same in the two frames due to the characteristic VBF kinematics. The VBF amplitudes are dominant in the collinear limit (4.18), where the vector-boson colliding axis (i.e. the z-axis in figure 3) is identical with the beam axis, and hence the $\Delta\phi_{12}$ distributions

JHEP07(2009)101

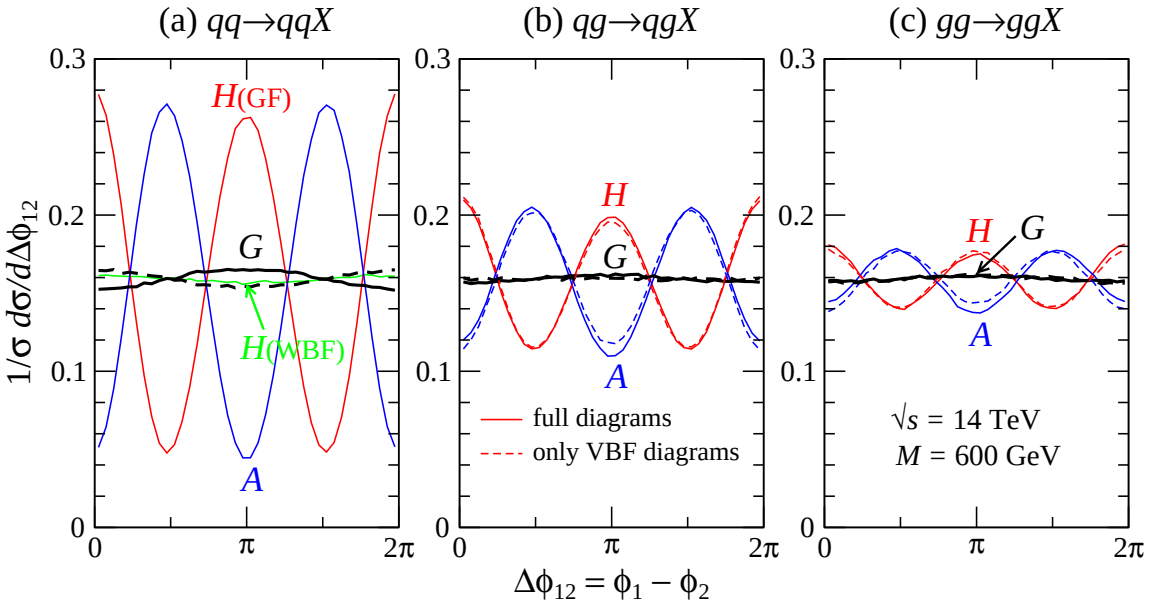

Figure 5. Normalized azimuthal correlations $\Delta\phi_{12}$ (mod 2π) between the two tagging jets in the $pp \to jjX$ process at the LHC, where the selection cuts (5.1) and (5.2) with $\Delta\eta_{jj\min} = 4$ are imposed. For the massive-graviton productions, the additional p_{T_j} cut (5.3) is also imposed. The distributions for each subprocess with the full diagrams (solid lines) and with the only VBF diagrams (dashed lines) are shown.

are not so much distorted. In fact, our $\Delta\phi_{12}$ distributions for the Higgs boson productions semi-quantitatively confirm those in the previous works [1–4].

Before turning to the spin-2 case, there are a few remarks related to the previous studies on the azimuthal correlations in the Hjj events. (i) The XVV coupling form factors are factorized as in eq. (5.13), and therefore, the $\Delta\phi_{12}$ distribution is insensitive to their effects [8]. (ii) As the ratio of the Higgs boson mass M to the partonic CM energy $\sqrt{\hat{s}}$ decreases, the interference effect grows [8]. In the collinear limit (4.18), we obtain

$$\frac{M^2}{\hat{s}} = \frac{-4\cos\theta_1\cos\theta_2}{(1+\cos\theta_1)(1-\cos\theta_2)} = z_1 z_2. \tag{5.17}$$

Therefore, as $M/\sqrt{\hat{s}}$ becomes smaller, i.e. $z_1 z_2 \to 0$, $\cos\theta_1$ and $\cos\theta_2$ approach zero, and the ratio of F_9^- to F_1 in eq. (5.10) grows; see eqs. (5.11) and (5.12). (iii) Although we have considered the three types of tensor structures separately for the Higgs coupling to vector bosons in this paper, it is easy to extend our analyses to a mixed CP scenario [3, 4, 10]; for instance, the additional phases, which come from the CP-mixed XVV coupling, can give rise to the *sine* terms in eq. (5.8), and explain the shift of the dip positions in figure 8 of ref. [4].

5.2.2 Massive graviton productions

Here, we discuss the case for the spin-2 particle productions, which is more involved than the scalar case, because all the nine amplitudes generically contribute to the total amplitude

JHEP07(2009)101

in eq. (2.7), which can lead all the 25 azimuthal distributions in eq. (5.5). Moreover, the graviton polarization along the momentum direction of the decay products (λ') depends on the decay angle Θ.

In section 5.1 we demonstrated that the QCD VBF amplitudes can have significant contribution to the G + 2-jet events by imposing the VBF cuts and the p_{T_j} slicing cut. In this case, the two off-shell VBF amplitudes, $\hat{\mathcal{M}}_{G\,+-}^{+2}$ and $\hat{\mathcal{M}}_{G\,-+}^{-2}$, are dominant, as mentioned in section 4.3. Therefore, only the F_9^+ ($\propto \mathcal{P}_{-+}^{+-}$) term in eq. (5.5) dominantly gives the nontrivial azimuthal correlation,

$$d\hat{\sigma}_G \sim \left[F_1 + 2\,F_9^+ \cos 2\Phi_{12}\right] \tag{5.18}$$

with $\Phi_{12} \equiv \phi_1 + \phi_2$. It should be emphasized here that Φ_{12} is not the azimuthal separation $\Delta\phi_{12}$ ($= \phi_1 - \phi_2$), but the sum of the azimuthal angles of the two jets, ϕ_1 and ϕ_2.

From (5.18), one can immediately conclude that the $\Delta\phi_{12}$ distributions for the massive-graviton productions are flat. In figure 5, the $\Delta\phi_{12}$ correlations for the KK graviton productions are also plotted with thick lines, where the p_{T_j} slicing cut (5.4) has been imposed as well as the inclusive cuts (5.1) and the VBF cuts (5.2).[8] The contributions from the $\lambda = \pm 1$ and 0 states, which can give rise to the $\cos\Delta\phi_{12}$ and $\cos 2\Delta\phi_{12}$ dependence in eq. (5.5), are invisibly small; they are smaller than the $\lambda = \pm 2$ by two and three orders of magnitude, respectively. The flat $\Delta\phi_{12}$ distribution for the massive-graviton productions is distinct from that for the SM Higgs boson productions, which is expected to have a dip around $\Delta\phi_{12} = \pi/2$ due to the GF contributions.

Now let us see the explicit forms of the functions F_1 and F_9^+ in eq. (5.18). From eq. (5.7) and by using the explicit forms of the amplitudes in tables 1(top), 2(top) and 5, one finds

$$\hat{F}_1^G[qq/qg/gg] = \hat{F}_1^H[qq/qg/gg] \times \frac{1}{2}\left\{\left(d^2_{+2,\lambda'}(\Theta)\right)^2 + \left(d^2_{-2,\lambda'}(\Theta)\right)^2\right\}, \tag{5.19}$$

$$\hat{F}_9^{+G}[qq/qg/gg] = \hat{F}_9^{-H}[qq/qg/gg] \times d^2_{+2,\lambda'}(\Theta)\, d^2_{-2,\lambda'}(\Theta), \tag{5.20}$$

where $\hat{F}_1^H$ and $\hat{F}_9^{-H}$ are the same as in eqs. (5.11) and (5.12), respectively, for the Higgs boson productions, and the common overall factor is

$$F_i^{(\pm)} = \frac{2g_s^4 g_{Ggg}^2 M^4 Q_1^2 Q_2^2}{\cos^2\theta_1 \cos^2\theta_2}\, \hat{F}_i^{(\pm)G}. \tag{5.21}$$

Here, from table 5, we take $\hat{\mathcal{M}}_{G\,\pm\mp}^{\pm 2} = -M^2$ in the collinear limit. By explicit forms of $J = 2$ d functions (see table 10), the functions in eqs. (5.19) and (5.20) are

$$\hat{F}_1^G[qq/qg/gg] = \hat{F}_1^H[qq/qg/gg] \times \begin{cases} \frac{1}{16}(1 + 6\cos^2\Theta + \cos^4\Theta) & \text{for } \lambda' = \pm 2, \\ \frac{1}{4}(1 - \cos^4\Theta) & \text{for } \lambda' = \pm 1, \\ \frac{3}{8}\sin^4\Theta & \text{for } \lambda' = 0, \end{cases} \tag{5.22}$$

[8] See also figure 2 in ref. [46], where $M_G = 1\,\text{TeV}$ and the different selection cuts are applied.

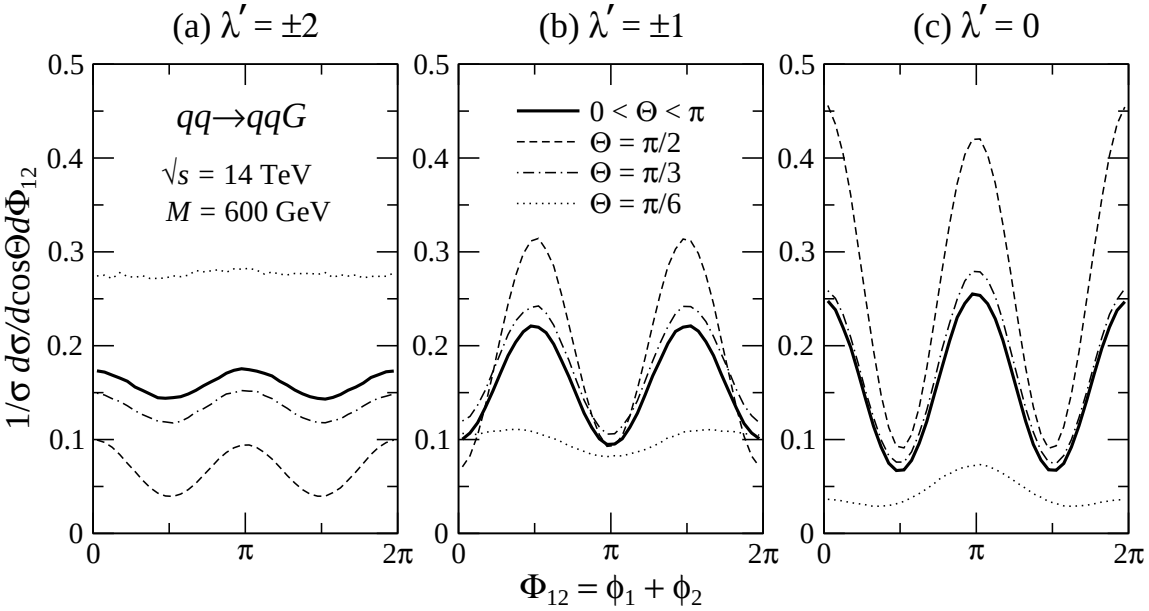

Figure 6. Azimuthal correlations Φ_{12} (mod 2π) between the two tagging jets for the qq-scattering subprocess in Gjj productions at the LHC, where the same selection cuts in figure 5 are imposed. The distributions for each final G polarization state, $\lambda' = \pm 2$ (a), ± 1 (b), and 0 (c), are shown at the decay angle $\Theta = \pi/2$ (dashed), $\pi/3$ (dashed-dotted), and $\pi/6$ (dotted), where they are normalized by $\sigma(pp \to jjG)\, B(G \to a_1' a_2')$. The distributions after integrating out Θ are also shown by thick solid lines.

and

$$\hat{F}_9^{+G}[qq/qg/gg] = \hat{F}_9^{-H}[qq/qg/gg] \times \begin{cases} \frac{1}{16}\sin^4\Theta & \text{for } \lambda' = \pm 2, \\ -\frac{1}{4}\sin^4\Theta & \text{for } \lambda' = \pm 1, \\ \frac{3}{8}\sin^4\Theta & \text{for } \lambda' = 0. \end{cases} \tag{5.23}$$

The distributions strongly depend on the decay angle Θ and the final polarization λ'. The Θ dependence is the same for $\lambda' = +2$ and -2, and also for $\lambda' = +1$ and -1. Since $J = 0$ resonances do not have such Θ dependence, the $J = 2$ and $\lambda' = 0$ state can be distinguished from the $J = \lambda' = 0$ state in principle. The coefficient function F_9^+ for all the final polarization states is proportional to $\sin^4\Theta$, and hence at $\Theta = 0$ and π, where the decay axis (z'-axis) is coincide with the initial polarization axis of the gravitons (z-axis), the azimuthal correlation is absent. This is because each colliding vector-boson has the definite helicity. Meanwhile, the correlation becomes larger with the larger decay angle, and reaches the maximum at $\Theta = \pi/2$, where the $\lambda = +2$ and -2 states are mixed maximally. It should be noted that the sign of the F_9^+ term for $\lambda' = \pm 1$ is different for the other states, which gives rise to the distinctive correlation.

JHEP07(2009)101

After integrating out the decay angle Θ, we obtain

$$\hat{F}_1^G[qq/qg/gg] = \hat{F}_1^H[qq/qg/gg] \times \frac{2}{5}\{1,\ 1,\ 1\} \qquad \text{for } \lambda' = \{\pm 2, \pm 1, 0\}, \tag{5.24}$$

$$\hat{F}_9^{+G}[qq/qg/gg] = \hat{F}_9^{-H}[qq/qg/gg] \times \frac{1}{15}\{1,\ -4,\ 6\} \qquad \text{for } \lambda' = \{\pm 2, \pm 1, 0\}. \tag{5.25}$$

The above results show that the magnitude of the azimuthal correlation depends on the final polarization λ'. The interference effect for the $\lambda' = 0$ case is largest among the possible five polarization states, although the decay branching ratio of KK gravitons into the $\lambda' = 0$ state, such as a pair of longitudinal weak-bosons and a $t\bar{t}$ pair with same helicities, is less than 1% for a whole mass range of gravitons. The correlation for $\lambda' = \pm 1$, which is realized in the decays into a fermion pair, is four times larger than that for $\lambda' = \pm 2$, which is projected out in the $G \to VV$ decays. It is worth noting that the above results depend only on λ', not on the decay mode. This universality of the angular correlation can be an experimental signal of the X spin measurement.

To examine the above analytic expectations, we demonstrate in figure 6 the azimuthal correlations Φ_{12} (mod 2π) between the two tagging jets for the qq-collision subprocess in Gjj events at the LHC, where the full diagrams are taken into account and the same selection cuts in figure 5 are imposed, i.e., the selection cuts (5.1), (5.2) and (5.3). The distributions for each final polarization state, $\lambda' = \pm 2$, ± 1, 0, are shown at the decay angle $\Theta = \pi/2$, $\pi/3$, and $\pi/6$, where they are normalized by $\sigma(pp \to jjG)\, B(G \to a_1' a_2')$. The distributions after integrating out Θ are also shown by thick solid lines, which is normalized to unity. The above analytical results can describe the simulations very well. For the qg- and gg-scattering cases, all the qualitative behaviors are same, but the interference effects diminish as in the $\Delta\phi_{12}$ correlations for the Higgs boson case in figure 5. It should be stressed here that the observation of the d function behavior, or the Θ dependence, is a measurement of the X spin, which can be strengthened by the azimuthal correlation between the tagging jets.

5.3 Correlations in the decay into a vector-boson pair

As mentioned in section 2, the processes of a heavy-particle decay into a vector-boson pair which subsequently decay into $\ell\bar{\ell}$, $q\bar{q}$, or gg are closely related to the VBF production processes. Here we discuss the X decay correlations between the two decay planes of the vector bosons by using the explicit helicity amplitudes, as in the production process.

To simplify the production part, we consider s-channel X productions in gg fusion or $q\bar{q}$ annihilation and its subsequent decays into four-body final states, namely $n = 0$ and $n' = 4$ in (2.17), so that the initial polarization of X along the z-axis can be fixed, $\lambda = \pm 2$, ± 1, or 0. In the following we take $\lambda = \bar{\lambda}$ and suppress the production density matrix in eq. (2.17).

For the X decay processes (2.10), the decay density matrix is given in eq. (2.19b) in terms of the decay tensor $\mathcal{D}^{\lambda_1' \lambda_2'}_{\bar{\lambda}_1' \bar{\lambda}_2'}$ of eq. (2.20b). Similar to the azimuthal angle distributions for the production in eq. (5.5), those for the decays into a vector-boson pair in eq. (2.17)

JHEP07(2009)101

are generally expressed by [53]

$$d^J_{\lambda,\lambda'} d^J_{\lambda,\bar{\lambda}'} \mathcal{D}^{\lambda'_1\lambda'_2}_{\bar{\lambda}'_1\bar{\lambda}'_2} = F'_1 + \big\{2\,\Re e\big[F'_2\cos\phi'_1 + F'_3\cos\phi'_2 + F'_4\cos 2\phi'_1 + F'_5\cos 2\phi'_2 + F'^{\pm}_6\cos(\phi'_1 \pm \phi'_2) + F'^{\pm}_7\cos(2\phi'_1 \pm \phi'_2) + F'^{\pm}_8\cos(\phi'_1 \pm 2\phi'_2) + F'^{\pm}_9\cos 2(\phi'_1 \pm \phi'_2)\big] + (\Re e \to \Im m,\ \cos \to \sin)\big\}. \tag{5.26}$$

Here, and in the following, summation over repeated indices $(\lambda'_1, \lambda'_2, \bar{\lambda}'_1, \bar{\lambda}'_2) = \pm, 0$ is implied, and ϕ'_i is the azimuthal angle between the decay plane of the vector boson and the X production plane ($gg/q\bar{q} \to X \to V'V'$) in the partonic CM frame; see also figure 3.

Because the azimuthal angle dependences of the quark and gluon current amplitudes are the same for each helicity combination (see tables 1(bottom) and 2(bottom)), and because the phase of the product of the two currents for $\sigma'_1 = -\sigma'_3$ and $\sigma'_2 = -\sigma'_4$ is (see eqs. (4.11) and (4.15))

$$\hat{\mathcal{J}}'^{\lambda'_1}_{1\,\sigma'_1,\sigma'_3=-\sigma'_1}\hat{\mathcal{J}}'^{\lambda'_2}_{2\,\sigma'_2,\sigma'_4=-\sigma'_2} \propto e^{i(\lambda'_1\phi'_1 - \lambda'_2\phi'_2)}, \tag{5.27}$$

the coefficients $F'^{(\pm)}_{1\text{-}9}$ for $(f\bar{f})(f\bar{f})$, $(f\bar{f})(gg)$ and $(gg)(gg)$ decays are given in terms of two d functions and the decay tensors $\mathcal{D}^{\lambda'_1\lambda'_2}_{\bar{\lambda}'_1\bar{\lambda}'_2}$ as

$$\begin{aligned}
F'_1 &= d^J_{\lambda,\lambda'_1-\lambda'_2} d^J_{\lambda,\lambda'_1-\lambda'_2} \mathcal{D}^{\lambda'_1\lambda'_2}_{\lambda'_1\lambda'_2},\\
F'_2 &= d^J_{\lambda,-\lambda'_2} d^J_{\lambda,1-\lambda'_2} \mathcal{D}^{0\lambda'_2}_{+\lambda'_2} + d^J_{\lambda,-1-\lambda'_2} d^J_{\lambda,-\lambda'_2} \mathcal{D}^{-\lambda'_2}_{0\lambda'_2},\\
F'_3 &= d^J_{\lambda,\lambda'_1-1} d^J_{\lambda,\lambda'_1} \mathcal{D}^{\lambda'_1+}_{\lambda'_1 0} + d^J_{\lambda,\lambda'_1} d^J_{\lambda,\lambda'_1+1} \mathcal{D}^{\lambda'_1 0}_{\lambda'_1-},\\
F'_4 &= d^J_{\lambda,-1-\lambda'_2} d^J_{\lambda,1-\lambda'_2} \mathcal{D}^{-\lambda'_2}_{+\lambda'_2},\\
F'_5 &= d^J_{\lambda,\lambda'_1-1} d^J_{\lambda,\lambda'_1+1} \mathcal{D}^{\lambda'_1+}_{\lambda'_1-},\\
F'^{\pm}_6 &= d^J_{\lambda,-1/1} d^J_{\lambda,1} \mathcal{D}^{0\pm}_{+0} + d^J_{\lambda,0} d^J_{\lambda,2/0} \mathcal{D}^{00}_{+\mp} + d^J_{\lambda,-2/0} d^J_{\lambda,0} \mathcal{D}^{-\pm}_{00} + d^J_{\lambda,-1} d^J_{\lambda,1/-1} \mathcal{D}^{-0}_{0\mp},\\
F'^{\pm}_7 &= d^J_{\lambda,-2/0} d^J_{\lambda,1} \mathcal{D}^{-\pm}_{+0} + d^J_{\lambda,-1} d^J_{\lambda,2/0} \mathcal{D}^{-0}_{+\mp},\\
F'^{\pm}_8 &= d^J_{\lambda,-1/1} d^J_{\lambda,2/0} \mathcal{D}^{0\pm}_{+\mp} + d^J_{\lambda,-2/0} d^J_{\lambda,1/-1} \mathcal{D}^{-\pm}_{0\mp},\\
F'^{\pm}_9 &= d^J_{\lambda,-2/0} d^J_{\lambda,2/0} \mathcal{D}^{-\pm}_{+\mp}.
\end{aligned} \tag{5.28}$$

We note that this relations can be also applied to the processes with the same-helicity currents, namely the cases for $\sigma'_1 = \sigma'_3$ and/or $\sigma'_2 = \sigma'_4$, which appear only in the $g^* \to gg$ currents; the same arguments in the production part can be applied (see below eq. (5.7)). We should note that, similar to eq. (5.7) for the VBF production processes, the Θ-dependent azimuthal angle correlations are manifestly expressed by quantum interference among different helicity states of the intermediate vector-bosons in eq. (5.28).

5.3.1 Higgs boson decays

The decay amplitudes (2.15) for scalar particles are the coherent sum of the three amplitudes in which the decaying vector-bosons have the same helicities ($\lambda'_1 = \lambda'_2$), and there is no Θ dependence, i.e. $d^{J=0}_{\lambda,\lambda'}(\Theta) = 1$ in eq. (5.26) (and in eq. (5.28)). Therefore, similar to

JHEP07(2009)101

the production case, the azimuthal angle correlation (5.26) for the $J = 0$ particle decays is reduced to

$$\mathcal{D}^{\lambda'_1\lambda'_2}_{\bar\lambda'_1\bar\lambda'_2} = F'_1 + \left\{2\,\Re e\left[F'^{-}_6 \cos\Delta\phi'_{12} + F'^{-}_9 \cos 2\Delta\phi'_{12}\right] + (\Re e \to \Im m,\ \cos \to \sin)\right\}, \quad (5.29)$$

where $\Delta\phi'_{12} \equiv \phi'_1 - \phi'_2$ is the angle between the two decay planes of the vector bosons.

The decay angular correlations have been extensively studied for the Higgs boson decays into the weak bosons, $H \to Z^{(*)}Z$, $W^{(*)}W$ [29–33]. It may be worth pointing that the F'^{-}_6 and F'^{-}_9 terms in eq. (5.29) can be observable for the Higgs boson mass $M_H < 400\,\mathrm{GeV}$ since the decays into a pair of transverse weak-bosons are not negligible compared to the decays into longitudinal ones, as shown in (4.34). F'^{-}_6 is very small for the $H \to ZZ$ decay, while it is large for the $H \to WW$ decay due to the P-odd nature [30, 34]. One can see detailed simulations for the LHC in refs. [31–33]. It must be recalled here that there is no azimuthal correlation between the two jets in the WBF Higgs productions as discussed in eq. (5.9).

Here we discuss the correlations for the Higgs boson decays into a virtual-gluon pair, $H/A \to g^*g^* \to (q\bar q)(q\bar q)$, $(q\bar q)(gg)$, or $(gg)(gg)$, in some detail. In the on-shell limit, or $Q'_{1,2} \to 0$, where the above decay processes via a virtual-gluon pair are dominant, only the transverse amplitudes ($\hat{\mathcal{M}}'_{H/A\pm\pm}$) contribute to the decay amplitudes both for the CP-even/odd Higgs boson decays. Moreover, due to the P-odd nature, the F'^{-}_6 term vanishes for the QCD processes as in the VBF processes. Therefore, only the F'^{-}_9 term in eq. (5.29) is relevant in this case.

From the relation in (5.28) and by using the explicit forms of the amplitudes in tables 1(bottom), 2(bottom) and 4, the coefficients F'_1 and F'^{-}_9 in eq. (5.29) for each decay process, $(q\bar q)(q\bar q)$, $(q\bar q)(gg)$ and $(gg)(gg)$, are expressed (except for the color factors) as

$$\hat F'_1[(q\bar q)(q\bar q)] = (1+\cos^2\theta'_1)(1+\cos^2\theta'_2), \quad (5.30a)$$

$$\hat F'_1[(q\bar q)(gg)] = \frac{1}{\sin^2\theta'_2}(1+\cos^2\theta'_1)(3+\cos^2\theta'_2)^2 \quad \text{or} \quad (1 \leftrightarrow 2), \quad (5.30b)$$

$$\hat F'_1[(gg)(gg)] = \frac{1}{\sin^2\theta'_1\sin^2\theta'_2}(3+\cos^2\theta'_1)^2(3+\cos^2\theta'_2)^2, \quad (5.30c)$$

and

$$\hat F'^{-}_9[(q\bar q)(q\bar q)/(gg)(gg)] = \pm\frac{1}{2}(1-\cos^2\theta'_1)(1-\cos^2\theta'_2), \quad (5.31a)$$

$$\hat F'^{-}_9[(q\bar q)(gg)] = \mp\frac{1}{2}(1-\cos^2\theta'_1)(1-\cos^2\theta'_2), \quad (5.31b)$$

where the upper (lower) sign corresponds to the CP-even (-odd) Higgs boson case. Here we take the $Q'_1, Q'_2 \ll M$ limit for the $X \to VV$ amplitudes, where the only surviving amplitudes are $|\hat{\mathcal{M}}'_{H/A\pm\pm}| = \frac{1}{2}M^2$, with the common overall factor

$$F'^{(\pm)}_i = \frac{1}{2}g^2_{H/Agg}g_s^4M^4Q'^{\,2}_1Q'^{\,2}_2\,\hat F'^{(\pm)}_i. \quad (5.32)$$

The constant term F'_1 has the different contributions from the $q\bar q$ decay and the gg decay and can be larger as the process involves the $g^* \to gg$ splitting. As in the production processes

with the helicity-flip currents, the same-helicity currents ($\sigma'_1 = \sigma'_3$ and/or $\sigma'_2 = \sigma'_4$), which appear only in the gluon currents, give rise only the constant piece, F'_1. The interference term F'^{-}_9, which receives the contribution only from the opposite-helicity currents ($\sigma'_1 = -\sigma'_3$ and $\sigma'_2 = -\sigma'_4$), is same except for sign in all the decay processes. This is because the relative sign between the different helicity states for the outgoing fermion and gluon current amplitudes is different; see tables 1(bottom) and 2(bottom), and because the relative phases between $\hat{\mathcal{J}}'^{\lambda'}_{1\sigma'_1,-\sigma'_1}$ and $\hat{\mathcal{J}}'^{\lambda'}_{2\sigma'_2,-\sigma'_2}$ for the quark currents (4.11) are different from those for the gluon currents (4.15).

Aside from the coupling constant, the double ($q\bar{q}$) decays via a pair of gluons are the same as the decays via a virtual-photon pair, $H/A \to \gamma^*\gamma^* \to (\ell\bar{\ell}/q\bar{q})(\ell\bar{\ell}/q\bar{q})$, and we expect the strong correlations as in the GF $qq \to qqH/A$ processes. On the other hand, the decay correlations for $(q\bar{q})(gg)$ and $(gg)(gg)$ are much smaller than those for $qg \to qgH/A$ and $gg \to ggH/A$ since the reduction factor from the gluon currents for the decays, $(3+\cos^2\theta'_i)^2$ in (5.30), can be much larger than that for the productions, $(1+3\cos^2\theta_i)^2$ in (5.11). This is well known as the knowledge of the QCD parton branching; a quark-antiquark pair from the gluon, $g^* \to q\bar{q}$, has the strong correlation between the gluon polarization and the decay plane, while for $g^* \to gg$ the correlation is weak [54]. It may be a challenging task to observe the azimuthal correlations between the QCD jets in the Higgs boson decays at the LHC. The quantitative study will be reported elsewhere.

5.3.2 Massive graviton decays

For the spin-2 particle decays, unlike the scalar particle decays, the nine amplitudes should be coherently summed in eq. (2.15) and may give rise to all the 25 azimuthal distributions in eq. (5.26).

In this article, we study the process of the graviton decays into a weak-boson pair at the LHC,

$$pp \to G \to WW/ZZ \to (f_1\bar{f}_3)(f_2\bar{f}_4). \tag{5.33}$$

This includes final four-charged-lepton signals, which may give a clean signal and allow a complete kinematical reconstruction at the LHC. The s-channel G production has two possible sources, gg fusion and $q\bar{q}$ annihilation, even though the gg contribution dominates the cross section for the graviton mass up to 3.4 TeV [19]. In the parton CM frame, the polarization of the produced gravitons is fixed along the beam axis (z-axis) at $\lambda = +2$ or -2 in gluon fusion, while at $\lambda = +1$ or -1 in $q\bar{q}$ annihilation. The two different production modes lead totally different angular Θ distributions, as we will see below.

As mentioned in section 4.3, in the heavy graviton mass limit ($\beta' = \sqrt{1-4m_V^2/M^2} \to 1$), only three $G \to VV$ amplitudes survive for the decays into on-shell weak-bosons; see table 6. In this limit, therefore, the azimuthal distributions in eq. (5.26) can be reduced to

$$d^2_{\lambda,\lambda'} d^2_{\bar{\lambda},\bar{\lambda}'} \mathcal{D}^{\lambda'_1\lambda'_2}_{\bar{\lambda}'_1\bar{\lambda}'_2} = F'_1 + 2\,F'^{+}_6 \cos\Phi'_{12} + 2\,F'^{+}_9 \cos 2\Phi'_{12} \tag{5.34}$$

with $\Phi'_{12} \equiv \phi'_1 + \phi'_2$. It should be stressed here that Φ'_{12} is not the angle between two decay planes $\Delta\phi'_{12}\,(= \phi'_1 - \phi'_2)$, but the sum of ϕ'_1 and ϕ'_2, which are measured separately from the graviton production plane.

From eq. (5.28) and by using the explicit forms of the helicity amplitudes in tables 1(bottom) and 6 and d functions in table 10, the complete angular distributions of eq. (5.34) are presented for $\lambda = \pm 2$ and ± 1 in appendix C. After integrating out θ_1' and θ_2' in (C.1) and (C.2), the Θ-dependent coefficients in eq. (5.34) are

$$\hat{F}_1' = 3 + 10\cos^2\Theta + 3\cos^4\Theta, \tag{5.35a}$$

$$\hat{F}_6'^{+} = \kappa_1\kappa_2 \frac{9\pi^2}{64}(1 - \cos^4\Theta), \tag{5.35b}$$

$$\hat{F}_9'^{+} = \frac{1}{4}\sin^4\Theta, \tag{5.35c}$$

for $\lambda = \pm 2$ (the gg initial state), and

$$\hat{F}_1' = 8 + 4\cos^2\Theta - 12\cos^4\Theta, \tag{5.36a}$$

$$\hat{F}_6'^{+} = -\kappa_1\kappa_2 \frac{9\pi^2}{16}\sin^2\Theta\cos^2\Theta, \tag{5.36b}$$

$$\hat{F}_9'^{+} = -\sin^4\Theta, \tag{5.36c}$$

for $\lambda = \pm 1$ (the $q\bar{q}$ initial state), where the common over all factor is

$$F_i'^{(\pm)} = \frac{1}{18} g_{GVV}^2 g_{V_1 f_1 f_3}^2 g_{V_2 f_2 f_4}^2 M^4 {Q_1'}^2 {Q_2'}^2 \hat{F}_i'^{(\pm)} \tag{5.37}$$

with $g_{V_i f_i f_{i+2}}^2 = \left(g_-^{V_i f_i f_{i+2}}\right)^2 + \left(g_+^{V_i f_i f_{i+2}}\right)^2$, and the combination of the Vff couplings κ_i is

$$\kappa_i = \left[\left(g_-^{V_i f_i f_{i+2}}\right)^2 - \left(g_+^{V_i f_i f_{i+2}}\right)^2\right] / g_{V_i f_i f_{i+2}}^2. \tag{5.38}$$

The Vff couplings are given in (4.3). The Θ distributions for the Φ_{12}'-independent term, F_1', are totally different between the two initial states due to the angular momentum conservation; a pair of vector bosons from the $\lambda = \pm 2$ gravitons tend to decay to the forward and backward directions, while the $\lambda = \pm 1$ gravitons are not allowed to decay into a vector-boson pair at $\Theta = 0$ and π (in the $\beta' = 1$ limit), where the momentum direction of the decaying vector-bosons (z'-axis) is coincide with the polarization axis of the gravitons (z-axis). On the other hand, all the azimuthal correlations, $F_6'^{+}$ and $F_9'^{+}$, disappear at $\Theta = 0$ and π since each decaying vector-boson has the definite helicity. The coefficient $F_6'^{+}$ takes the maximum at $\Theta = \pi/2$ ($\pi/4$) for $\lambda = \pm 2$ (± 1), while the $F_9'^{+}$ becomes larger with the larger decay angle and reaches the maximum at $\Theta = \pi/2$ both for $\lambda = \pm 2$ and ± 1. The sign difference of the Φ_{12}'-dependent terms between $\lambda = \pm 2$ and ± 1 gives rise to the distinctive correlations.

Let us estimate the asymmetries $A_i \equiv 2F_i'^{+}/F_1'$ ($i = 6, 9$) from (5.35) and (5.36) for the $G \to ZZ \to 4\ell$ process. After the integration for Θ, one finds

$$A_6 = \kappa_1\kappa_2 \frac{27\pi^2}{832} \sim 0.007, \qquad A_9 = \frac{1}{26} \sim 0.038 \qquad \text{for } \lambda = \pm 2, \tag{5.39}$$

$$A_6 = -\kappa_1\kappa_2 \frac{9\pi^2}{416} \sim -0.005, \qquad A_9 = -\frac{2}{13} \sim -0.154 \qquad \text{for } \lambda = \pm 1. \tag{5.40}$$

JHEP07(2009)101

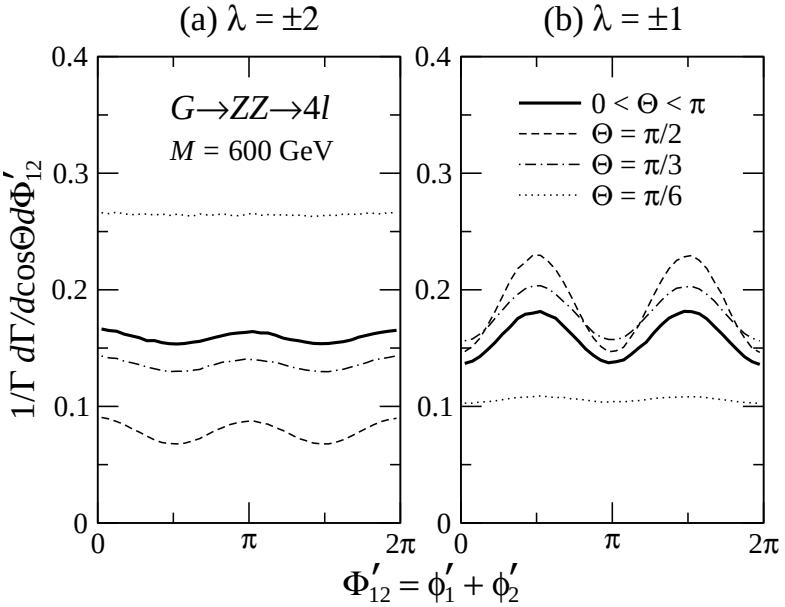

Figure 7. Normalized azimuthal correlations Φ'_{12} (mod 2π) between the decay planes of the vector bosons in the $G \to ZZ \to 4\ell$ decays for the initial helicity $\lambda = \pm 2$ (a) and ± 1 (b), where the decay angle Θ is fixed at $\pi/2$ (dashed), $\pi/3$ (dashed-dotted), and $\pi/6$ (dotted). The distributions after integrating out Θ are also shown by thick solid lines.

The asymmetry A_6 of the $\cos\Phi'_{12}$ term is tiny both for $\lambda = \pm 2$ and ± 1, less than 1%, due to the smallness of the parity violation for the Z decays, similar to the $H \to ZZ \to 4\ell$ process. On the other hand, A_9 of the $\cos 2\Phi'_{12}$ term reaches around 4% for $\lambda = \pm 2$ and 15% for $\lambda = \pm 1$.

We simulate the $G \to ZZ \to 4\ell$ process to examine our analytic expectations, where we take $M = 600\,\text{GeV}$, $m_Z = 91.2\,\text{GeV}$ and $\Gamma_Z = 2.5\,\text{GeV}$, that is, all the nine amplitudes in (2.15) are taken into account without any approximation. Figure 7 shows the normalized azimuthal correlations Φ'_{12} (mod 2π) between the decay planes of the vector bosons for $\lambda = \pm 2$ (a) and ± 1 (b). The decay angle Θ is fixed at $\pi/2$, $\pi/3$, and $\pi/6$, shown by dashed, dashed-dotted, and dotted lines, respectively. The distributions after integrating out Θ are also shown by thick solid lines, which are normalized to unity. Our analytic approximation can explain the results not only qualitatively but also quantitatively. It should be stressed again that the observation of the Θ dependence of the azimuthal correlations can be a measurement of the X spin.

At the LHC, as mentioned before, gg fusion is the main production process of KK gravitons, that is, the $\lambda = \pm 2$ states are mainly produced. Therefore, the azimuthal distribution is expected to be suppressed around $\Phi'_{12} = \pi/2$. However, for the higher graviton mass region, the contribution from $q\bar{q}$ annihilation, which enhance the events around $\Phi'_{12} = \pi/2$, becomes larger and gives rise to cancel the correlation each other. At the graviton mass $M = 3.4\,\text{TeV}$ the production rate of the two contributions is comparable [19], and hence the azimuthal distributions are enhanced around $\Phi'_{12} = \pi/2$ since the correlation in $q\bar{q}$ annihilation is stronger than that in gluon fusion; see (5.39) and (5.40).

JHEP07(2009)101

In the future e^+e^- (or photon) linear collider, on the other hand, only the $\lambda = \pm 1$ (or $\lambda = \pm 2$) state can be produced, and more precise studied to determine the spin-2 nature may be done in the clean environment.

6 Summary

We have studied angular correlations of the two accompanying jets in Higgs boson and massive-graviton productions at hadron colliders, which include WBF and GF processes. We have also considered their decays into a vector-boson pair which subsequently decay into $\ell\bar{\ell}$, $q\bar{q}$ or gg.

The amplitudes for the VBF subprocesses are given by the product of the two incoming current amplitudes and the off-shell $VV \to X$ amplitude summed over the polarization of the t-channel intermediate vector-bosons (see eq. (2.7)), while the amplitudes for the X decays into four final states via a vector-boson pair are expressed as the product of the $X \to VV$ amplitude and the two outgoing current amplitudes summed over the polarization of the s-channel intermediate vector-bosons (see eq. (2.15)). Using the kinematical variables in figure 3, we presented all the helicity amplitudes explicitly; tables 1 and 2 for the quark and gluon currents, and tables 4 and 5 for the $VV \to H/A$ and $VV \to G$ processes, respectively. We also showed that our off-shell vector-boson current amplitudes reduce to the standard quark and gluon splitting amplitudes with appropriate gluon-polarization phases in the collinear limit (eqs. (4.18) and (4.20)).

To validate our analyses, we demonstrated that the VBF amplitudes dominate the exact matrix elements not only for the WBF processes but also for all the GF processes when typical selection cuts to enhance the VBF events are applied, such as a large rapidity separation between two jets in (5.2). Furthermore, we found that the p_{Tj} slicing cut (5.4) is effective to suppress the non-VBF diagrams especially for the graviton productions.

By using the density matrix formalism in eq. (2.17) and our analytical amplitudes, we showed that nontrivial azimuthal angle correlations of the jets in the production and in the decay of massive spin-0 and -2 bosons are manifestly expressed in terms of the quantum interference among different helicity states of the intermediate vector-bosons; see (5.7) for the production and (5.28) for the decay.

For the productions and the decays of Higgs bosons, our analytical arguments can describe the previous studies on the angular correlations; for instance, the WBF gives the flat azimuthal distribution (5.9), while the GF produces the $\cos 2(\phi_1 - \phi_2)$ distribution (5.10). We also explicitly showed that the gluon currents, especially in the decay processes, reduce the azimuthal correlations. For the massive-graviton case, we found the Θ-dependent $\cos 2(\phi_1 + \phi_2)$ correlations for both the production processes (5.18) and the decay processes (5.34), which are proportional to $\sin^4\Theta$. The correlations also depend on the final graviton polarization in the productions and on the initial graviton polarization in the decays. Those correlations reflect the spin and the CP nature of the Higgs bosons and the massive gravitons, and may have a great potential to be observed at the LHC.

JHEP07(2009)101

Acknowledgments

We wish to thank Y. Matsumoto and D. Nomura for discussions in the early stage of the investigation. Q.L. and K.M. would like to thank the KEK theory group for the warm hospitality, and also the IPMU (Institute for Physics and Mathematics of the Universe) for organizing LHC focus week meetings in December 2007 and March 2009 where we enjoyed stimulating discussions. K.H. and K.M. would like to thank the Aspen Center for Physics and program: "LHC: Beyond the Standard Model Signals in a QCD Environment" where a part of this work was done. K.M. also thanks O. Nachtmann, T. Plehn and S. Schumann for valuable comments. This work is supported in part by the Core University Program of JSPS, and in part by the Grant-in-Aid for Scientific Research (No. 20340064) from MEXT, Japan.

The diagrams in this paper were drawn using `JaxoDraw` [55].

A Wavefunction and vertices for a spin-2 particle

The polarization tensor for a spin-2 particle in table 3, $\epsilon^{\mu\nu}(p,\lambda)$, is decomposed into polarization vectors for a spin-1 particle as

$$\begin{aligned}
\epsilon^{\mu\nu}(p,\pm 2) &= \epsilon^{\mu}(p,\pm)\,\epsilon^{\nu}(p,\pm),\\
\epsilon^{\mu\nu}(p,\pm 1) &= \frac{1}{\sqrt{2}}\big[\epsilon^{\mu}(p,\pm)\,\epsilon^{\nu}(p,0)+\epsilon^{\mu}(p,0)\,\epsilon^{\nu}(p,\pm)\big],\\
\epsilon^{\mu\nu}(p,0) &= \frac{1}{\sqrt{6}}\big[\epsilon^{\mu}(p,+)\,\epsilon^{\nu}(p,-)+\epsilon^{\mu}(p,-)\,\epsilon^{\nu}(p,+)+2\,\epsilon^{\mu}(p,0)\,\epsilon^{\nu}(p,0)\big].
\end{aligned} \tag{A.1}$$

See more details in ref. [46].

The vertices for a massive graviton with two vector-bosons in table 3 are given by [56]

$$\hat{\Gamma}^{\mu\nu,\alpha\beta}_{GVV}(q_1,q_2) = (m_V^2+q_1\cdot q_2)\,C^{\mu\nu,\alpha\beta}+D^{\mu\nu,\alpha\beta}(q_1,q_2)+\xi^{-1}E^{\mu\nu,\alpha\beta}(q_1,q_2), \tag{A.2}$$

where $q_{1,2}$ and m_V are the momenta and mass of the vector bosons, and

$$C^{\mu\nu,\alpha\beta} = g^{\mu\alpha}g^{\nu\beta}+g^{\mu\beta}g^{\nu\alpha}-g^{\mu\nu}g^{\alpha\beta}, \tag{A.3}$$

$$D^{\mu\nu,\alpha\beta}(q_1,q_2) = g^{\mu\nu}q_1^{\beta}q_2^{\alpha}-\big[g^{\mu\beta}q_1^{\nu}q_2^{\alpha}+g^{\mu\alpha}q_1^{\beta}q_2^{\nu}-g^{\alpha\beta}q_1^{\mu}q_2^{\nu}+(\mu\leftrightarrow\nu)\big], \tag{A.4}$$

$$E^{\mu\nu,\alpha\beta}(q_1,q_2) = g^{\mu\nu}(q_1^{\alpha}q_1^{\beta}+q_2^{\alpha}q_2^{\beta}+q_1^{\alpha}q_2^{\beta})-\big[g^{\nu\beta}q_1^{\mu}q_1^{\alpha}+g^{\nu\alpha}q_2^{\mu}q_2^{\beta}+(\mu\leftrightarrow\nu)\big]. \tag{A.5}$$

The ξ term is the gauge-fixing term, which vanishes for massive vector-bosons in the unitary gauge ($\xi\to\infty$). For massless vector-bosons we take $\xi=1$ in the Feynman gauge.

B Relation between wavefunctions and d functions

In this appendix, we demonstrate that two-to-two processes via s-channel spin-2 resonances can be factorized into the production part and its decay part, by using explicit spin-2 wavefunctions. In the resonance (X) rest frame, $p^{\mu}=(m,\vec{0})$, we consider the processes

$$a_1(k_1,\sigma_1)+a_2(k_2,\sigma_2)\to X(p)\to a_1'(k_1',\sigma_1')+a_2'(k_2',\sigma_2'), \tag{B.1}$$

where the a_1 momentum (k_1) is taken along the positive z-axis and the a_1' momentum (k_1') is given by the scattering angle θ.

Before we consider the spin-2 resonance case, let us start with the well-known spin-1 case. The numerator of the propagator for spin-1 particles,

$$P^{\mu\nu}(p) = g^{\mu\nu} - \frac{p^\mu p^\nu}{p^2} = -\sum_{\lambda=\pm1,0} \epsilon^\mu(p,\lambda)^*\,\epsilon^\nu(p,\lambda), \tag{B.2}$$

is a projector on the on-shell particle, $p^2 = m^2$. Since the projector is an operator which satisfies $P^2 = P$, namely

$$\begin{aligned} P^{\mu\nu}(p) &= P^{\mu\rho}(p) P_\rho{}^\nu(p) \\ &= \sum_\lambda \epsilon^\mu(p,\lambda)^*\,\epsilon^\rho(p,\lambda) \sum_{\lambda'} \epsilon_\rho(p,\lambda')^*\,\epsilon^\nu(p,\lambda'). \end{aligned} \tag{B.3}$$

Here, λ is the helicity along the incoming a_1 momentum and λ' is the helicity along the outgoing a_1' momentum, that is, $\lambda = \sigma_1 - \sigma_2$ and $\lambda' = \sigma_1' - \sigma_2'$. On the mass-shell, the propagator factor (B.3) can be factorized into the production part and the decay part; the wavefunction $\epsilon^\mu(p,\lambda)^*$ is used to calculate the production amplitudes, and the wavefunction $\epsilon^\nu(p,\lambda')$ is used to calculate the decay amplitudes. There is a connecting factor, $\epsilon^\rho(p,\lambda)\,\epsilon_\rho(p,\lambda')^*$, which should be a scalar function depending on λ, λ', and the orientation angle θ between the two quantization axes. Using the explicit forms of the spin-1 polarization vectors (with the HELAS convention [38]):

$$\begin{aligned} \epsilon^\mu(p,\lambda=\pm) &= \frac{1}{\sqrt{2}}(0,\,\mp1,\,-i,\,0), \\ \epsilon^\mu(p,\lambda=0) &= (0,\,0,\,0,\,1), \end{aligned} \tag{B.4}$$

and

$$\begin{aligned} \epsilon^\mu(p,\lambda'=\pm) &= \frac{1}{\sqrt{2}}(0,\,\mp\cos\theta,\,-i,\,\pm\sin\theta), \\ \epsilon^\mu(p,\lambda'=0) &= (0,\,\sin\theta,\,0,\,\cos\theta), \end{aligned} \tag{B.5}$$

the connecting factor can be expressed as the $J=1$ d function,

$$\epsilon^\rho(p,\lambda)\,\epsilon_\rho(p,\lambda')^* = -\begin{bmatrix} \frac{1}{2}(1+\cos\theta) & -\frac{1}{\sqrt{2}}\sin\theta & \frac{1}{2}(1-\cos\theta) \\ \frac{1}{\sqrt{2}}\sin\theta & \cos\theta & -\frac{1}{\sqrt{2}}\sin\theta \\ \frac{1}{2}(1-\cos\theta) & \frac{1}{\sqrt{2}}\sin\theta & \frac{1}{2}(1+\cos\theta) \end{bmatrix} = -d^1_{\lambda,\lambda'}(\theta). \tag{B.6}$$

The d function dictates the overlap of the angular momentum states between the initial a_1a_2 and the final $a_1'a_2'$ state. Finally, the propagator factor (B.3) can be rewritten as

$$P^{\mu\nu}(p) = -\sum_{\lambda,\lambda'} \epsilon^\mu(p,\lambda)^*\, d^1_{\lambda,\lambda'}(\theta)\,\epsilon^\nu(p,\lambda'). \tag{B.7}$$

Note that the sign comes from the orthogonal relation, $\epsilon^\mu(p,\lambda^{(\prime)})\,\epsilon_\mu(p,\lambda^{(\prime)})^* = -1$.

JHEP07(2009)101

$d^2_{\pm 2,2} = d^2_{\mp 2,-2}$	$\frac{1}{4}(1 \pm \cos\theta)^2$		
$d^2_{\pm 2,1} = -d^2_{\mp 2,-1}$	$\mp\frac{1}{2}(1 \pm \cos\theta)\sin\theta$	$d^2_{\pm 1,1} = d^2_{\mp 1,-1}$	$\frac{1}{2}(1 \pm \cos\theta)(2\cos\theta \mp 1)$
$d^2_{\pm 2,0}$	$\frac{\sqrt{6}}{4}\sin^2\theta$	$d^2_{\pm 1,0}$	$\mp\frac{\sqrt{6}}{2}\sin\theta\cos\theta$

Table 10. Explicit forms of $J = 2$ d functions.

Now, let us move to the spin-2 case. Similarly, the propagator factor for spin-2 particles is a projector on the mass-shell ($p^2 = m^2$):

$$\begin{aligned} P^{\mu\nu\alpha\beta}(p) &= \frac{1}{2}(g^{\mu\alpha}g^{\nu\beta} + g^{\mu\beta}g^{\nu\alpha} - g^{\mu\nu}g^{\alpha\beta}) \\ &\quad - \frac{1}{2p^2}(g^{\mu\alpha}p^\nu p^\beta + g^{\nu\beta}p^\mu p^\alpha + g^{\mu\beta}p^\nu p^\alpha + g^{\nu\alpha}p^\mu p^\beta) \\ &\quad + \frac{1}{6}\Big(g^{\mu\nu} + \frac{2}{p^2}p^\mu p^\nu\Big)\Big(g^{\alpha\beta} + \frac{2}{p^2}p^\alpha p^\beta\Big) \\ &= \sum_{\lambda=\pm 2,\pm 1,0} \epsilon^{\mu\nu}(p,\lambda)^*\epsilon^{\alpha\beta}(p,\lambda), \end{aligned} \tag{B.8}$$

where $\epsilon^{\mu\nu}(p,\lambda)$ is a spin-2 wavefunction. On the mass-shell, the summation over the helicity can be duplicated,

$$\begin{aligned} P^{\mu\nu\alpha\beta}(p) &= P^{\mu\nu\rho\sigma}(p)P_{\rho\sigma}{}^{\alpha\beta}(p) \\ &= \sum_\lambda \epsilon^{\mu\nu}(p,\lambda)^*\,\epsilon^{\rho\sigma}(p,\lambda)\sum_{\lambda'}\epsilon_{\rho\sigma}(p,\lambda')^*\,\epsilon^{\alpha\beta}(p,\lambda'). \end{aligned} \tag{B.9}$$

By using the explicit forms of the spin-2 polarization tensors in eq. (A.1) and the polarization vectors in eqs. (B.4) and (B.5), one finds that the overlap factor is the $J = 2$ d function (see table 10) as

$$\epsilon^{\rho\sigma}(p,\lambda)\,\epsilon_{\rho\sigma}(p,\lambda')^* = d^2_{\lambda,\lambda'}(\theta). \tag{B.10}$$

Therefore, the propagator factor for spin-2 particles (B.9) can be factorized into the production and the decay part as

$$P^{\mu\nu\alpha\beta}(p) = \sum_{\lambda,\lambda'}\epsilon^{\mu\nu}(p,\lambda)^*\,d^2_{\lambda,\lambda'}(\theta)\,\epsilon^{\alpha\beta}(p,\lambda'). \tag{B.11}$$

C Angular distributions for $G \to VV \to (f\bar{f})(f\bar{f})$

In the heavy graviton mass limit $\left(\beta' = \sqrt{1 - 4m_V^2/M^2} \to 1\right)$, where the only three amplitudes among the nine $G \to VV$ amplitudes in table 6 are relevant, the differential distribution of the massive-graviton decays, $G \to VV \to (f_1\bar{f}_3)(f_2\bar{f}_4)$, for the initial polarization

$\lambda = \pm 2$ along the z-axis is given by the expression

$$\begin{aligned}
&\frac{d\Gamma_G^{\lambda=\pm 2}}{d\cos\Theta\, d\cos\theta_1\, d\cos\theta_2\, d\Phi_{12}} \\
&\quad \sim (1+6c^2+c^4)\{(1+c_1^2)(1+c_2^2)+4\kappa_1\kappa_2 c_1 c_2\} + 2s^4 s_1^2 s_2^2 \\
&\qquad \mp 8c(1+c^2)\{\kappa_1 c_1(1+c_2^2)+\kappa_2(1+c_1^2)c_2\} \\
&\qquad + 4s^2 s_1 s_2\{(1+c^2)(\kappa_1\kappa_2+c_1c_2) \mp 2c(\kappa_2 c_1+\kappa_1 c_2)\}\cos\Phi_{12} \\
&\qquad + s^4 s_1^2 s_2^2 \cos 2\Phi_{12}
\end{aligned} \tag{C.1}$$

with $\Phi_{12} = \phi_1 + \phi_2$, the abbreviations $c = \cos\Theta$, $s = \sin\Theta$, $c_i = \cos\theta_i$ and $s_i = \sin\theta_i$, and κ_i in eq. (5.38); see figure 3 for the definition of the kinematical variables. Here, primes ($'$) which indicate the decay variables in the text are omitted for simplicity. For the $\lambda = \pm 1$ state, the distribution reads

$$\begin{aligned}
&\frac{d\Gamma_G^{\lambda=\pm 1}}{d\cos\Theta\, d\cos\theta_1\, d\cos\theta_2\, d\Phi_{12}} \\
&\quad \sim 4(1-c^4)\{(1+c_1^2)(1+c_2^2)+4\kappa_1\kappa_2 c_1 c_2\} + 8s^2 c^2 s_1^2 s_2^2 \\
&\qquad \mp 16c(1-c^2)\{\kappa_1 c_1(1+c_2^2)+\kappa_2(1+c_1^2)c_2\} \\
&\qquad - 16s^2 c s_1 s_2[c(\kappa_1\kappa_2+c_1c_2) \mp (\kappa_2 c_1+\kappa_1 c_2)]\cos\Phi_{12} \\
&\qquad - 4s^4 s_1^2 s_2^2 \cos 2\Phi_{12},
\end{aligned} \tag{C.2}$$

where the same normalization is used as in eq. (C.1).

References

[1] T. Plehn, D.L. Rainwater and D. Zeppenfeld, *Determining the structure of Higgs couplings at the LHC*, *Phys. Rev. Lett.* **88** (2002) 051801 [hep-ph/0105325] [SPIRES].

[2] V. Del Duca, W. Kilgore, C. Oleari, C. Schmidt and D. Zeppenfeld, *H + 2 jets via gluon fusion*, *Phys. Rev. Lett.* **87** (2001) 122001 [hep-ph/0105129] [SPIRES]; *Gluon-fusion contributions to H + 2 jet production*, *Nucl. Phys.* **B 616** (2001) 367 [hep-ph/0108030] [SPIRES].

[3] V. Hankele, G. Klamke and D. Zeppenfeld, *Higgs + 2 jets as a probe for CP properties*, hep-ph/0605117 [SPIRES].

[4] G. Klamke and D. Zeppenfeld, *Higgs plus two jet production via gluon fusion as a signal at the CERN LHC*, *JHEP* **04** (2007) 052 [hep-ph/0703202] [SPIRES].

[5] T. Arens, O. Nachtmann, M. Diehl and P.V. Landshoff, *Some tests for the helicity structure of the Pomeron in e p collisions*, *Z. Phys.* **C 74** (1997) 651 [hep-ph/9605376] [SPIRES].

[6] F.E. Close and G.A. Schuler, *Central production of mesons: Exotic states versus Pomeron structure*, *Phys. Lett.* **B 458** (1999) 127 [hep-ph/9902243] [SPIRES];
F.E. Close, A. Kirk and G. Schuler, *Dynamics of glueball and q anti-q production in the central region of p p collisions*, *Phys. Lett.* **B 477** (2000) 13 [hep-ph/0001158] [SPIRES].

[7] A.B. Kaidalov, V.A. Khoze, A.D. Martin and M.G. Ryskin, *Central exclusive diffractive production as a spin parity analyser: From hadrons to Higgs*, *Eur. Phys. J.* **C 31** (2003) 387 [hep-ph/0307064] [SPIRES].

JHEP07(2009)101

[8] T. Figy and D. Zeppenfeld, *QCD corrections to jet correlations in weak boson fusion*, *Phys. Lett.* **B 591** (2004) 297 [hep-ph/0403297] [SPIRES].

[9] J.M. Campbell, R.K. Ellis and G. Zanderighi, *Next-to-leading order Higgs + 2 jet production via gluon fusion*, *JHEP* **10** (2006) 028 [hep-ph/0608194] [SPIRES].

[10] V. Hankele, G. Klamke, D. Zeppenfeld and T. Figy, *Anomalous Higgs boson couplings in vector boson fusion at the CERN LHC*, *Phys. Rev.* **D 74** (2006) 095001 [hep-ph/0609075] [SPIRES].

[11] M. Ciccolini, A. Denner and S. Dittmaier, *Strong and electroweak corrections to the production of Higgs+2jets via weak interactions at the LHC*, *Phys. Rev. Lett.* **99** (2007) 161803 [arXiv:0707.0381] [SPIRES]; *Electroweak and QCD corrections to Higgs production via vector-boson fusion at the LHC*, *Phys. Rev.* **D 77** (2008) 013002 [arXiv:0710.4749] [SPIRES].

[12] J.R. Andersen, T. Binoth, G. Heinrich and J.M. Smillie, *Loop induced interference effects in Higgs Boson plus two jet production at the LHC*, *JHEP* **02** (2008) 057 [arXiv:0709.3513] [SPIRES].

[13] J.R. Andersen, V. Del Duca and C.D. White, *Higgs Boson Production in Association with Multiple Hard Jets*, *JHEP* **02** (2009) 015 [arXiv:0808.3696] [SPIRES].

[14] K. Odagiri, *On azimuthal spin correlations in Higgs plus jet events at LHC*, *JHEP* **03** (2003) 009 [hep-ph/0212215] [SPIRES].

[15] V. Del Duca et al., *Monte Carlo studies of the jet activity in Higgs + 2jet events*, *JHEP* **10** (2006) 016 [hep-ph/0608158] [SPIRES].

[16] L. Randall and R. Sundrum, *A large mass hierarchy from a small extra dimension*, *Phys. Rev. Lett.* **83** (1999) 3370 [hep-ph/9905221] [SPIRES]; *An alternative to compactification*, *Phys. Rev. Lett.* **83** (1999) 4690 [hep-th/9906064] [SPIRES].

[17] H. Davoudiasl, J.L. Hewett and T.G. Rizzo, *Phenomenology of the Randall-Sundrum Gauge Hierarchy Model*, *Phys. Rev. Lett.* **84** (2000) 2080 [hep-ph/9909255] [SPIRES]; *Experimental probes of localized gravity: On and off the wall*, *Phys. Rev.* **D 63** (2001) 075004 [hep-ph/0006041] [SPIRES].

[18] B.C. Allanach, K. Odagiri, M.A. Parker and B.R. Webber, *Searching for narrow graviton resonances with the ATLAS detector at the Large Hadron Collider*, *JHEP* **09** (2000) 019 [hep-ph/0006114] [SPIRES].

[19] B.C. Allanach et al., *Exploring small extra dimensions at the large hadron collider*, *JHEP* **12** (2002) 039 [hep-ph/0211205] [SPIRES].

[20] P. Traczyk and G. Wrochna, *Search for Randall-Sundrum graviton excitations in the CMS experiment*, hep-ex/0207061 [SPIRES];
I. Belotelov et al., *Search for Randall-Sundrum graviton decay into muon pairs*, CERN-CMS-NOTE-2006-104 [SPIRES] and references therein.

[21] P. Osland, A.A. Pankov and N. Paver, *Discriminating graviton exchange effects from other new physics scenarios in e^+e^- collisions*, *Phys. Rev.* **D 68** (2003) 015007 [hep-ph/0304123] [SPIRES];
E.W. Dvergsnes, P. Osland, A.A. Pankov and N. Paver, *Center edge asymmetry at hadron colliders*, *Phys. Rev.* **D 69** (2004) 115001 [hep-ph/0401199] [SPIRES];

JHEP07(2009)101

P. Osland, A.A. Pankov, N. Paver and A.V. Tsytrinov, *Spin identification of the Randall-Sundrum resonance in lepton-pair production at the LHC*, *Phys. Rev.* **D 78** (2008) 035008 [arXiv:0805.2734] [SPIRES].

[22] R. Cousins, J. Mumford, J. Tucker and V. Valuev, *Spin discrimination of new heavy resonances at the LHC*, *JHEP* **11** (2005) 046 [SPIRES].

[23] P. Mathews and V. Ravindran, *Angular distribution of Drell-Yan process at hadron colliders to NLO-QCD in models of TeV scale gravity*, *Nucl. Phys.* **B 753** (2006) 1 [hep-ph/0507250] [SPIRES].

[24] D0 collaboration, V.M. Abazov et al., *Search for Randall-Sundrum gravitons in dilepton and diphoton final states*, *Phys. Rev. Lett.* **95** (2005) 091801 [hep-ex/0505018] [SPIRES];
CDF collaboration, A. Abulencia et al., *Search for new high mass particles decaying to lepton pairs in $p\bar{p}$ collisions at $\sqrt{s} = 1.96$ TeV*, *Phys. Rev. Lett.* **95** (2005) 252001 [hep-ex/0507104] [SPIRES].

[25] H. Murayama and V. Rentala, *Randall-Sundrum graviton spin determination using azimuthal angular dependence*, arXiv:0904.4561 [SPIRES].

[26] N. Arkani-Hamed, S. Dimopoulos and G.R. Dvali, *The hierarchy problem and new dimensions at a millimeter*, *Phys. Lett.* **B 429** (1998) 263 [hep-ph/9803315] [SPIRES];
I. Antoniadis, N. Arkani-Hamed, S. Dimopoulos and G.R. Dvali, *New dimensions at a millimeter to aFermi and superstrings at a TeV*, *Phys. Lett.* **B 436** (1998) 257 [hep-ph/9804398] [SPIRES];
N. Arkani-Hamed, S. Dimopoulos and G.R. Dvali, *Phenomenology, astrophysics and cosmology of theories with sub-millimeter dimensions and TeV scale quantum gravity*, *Phys. Rev.* **D 59** (1999) 086004 [hep-ph/9807344] [SPIRES].

[27] K. Hagiwara, P. Konar, Q. Li, K. Mawatari and D. Zeppenfeld, *Graviton production with 2 jets at the LHC in large extra dimensions*, *JHEP* **04** (2008) 019 [arXiv:0801.1794] [SPIRES].

[28] L.D. Landau, *On the angular moment of a two-photon system*, *Dokl. Akad. Nawk. USSR* **60** (1948) 207;
C.-N. Yang, *Selection Rules for the Dematerialization of a Particle Into Two Photons*, *Phys. Rev.* **77** (1950) 242 [SPIRES].

[29] J.R. Dell'Aquila and C.A. Nelson, *P or CP determination by sequential decays: V1 V2 modes with decays into anti-lepton (A) lepton (B) and/or anti-q (A) q (B)*, *Phys. Rev.* **D 33** (1986) 80 [SPIRES];
C.A. Nelson, *Correlation between decay planes in Higgs boson decays into W pair (into Z pair)*, *Phys. Rev.* **D 37** (1988) 1220 [SPIRES].

[30] A. Skjold and P. Osland, *Angular and energy correlations in Higgs decay*, *Phys. Lett.* **B 311** (1993) 261 [hep-ph/9303294] [SPIRES];
V.D. Barger, K.-m. Cheung, A. Djouadi, B.A. Kniehl and P.M. Zerwas, *Higgs bosons: Intermediate mass range at e^+e^- colliders*, *Phys. Rev.* **D 49** (1994) 79 [hep-ph/9306270] [SPIRES].

[31] M. Hohlfeld, *On the determination of Higgs parameters in the ATLAS experiment at the LHC*, ATLAS Report ATL-PHYS-2001-004 (2001).

[32] S.Y. Choi, . Miller, D. J., M.M. Muhlleitner and P.M. Zerwas, *Identifying the Higgs spin and parity in decays to Z pairs*, *Phys. Lett.* **B 553** (2003) 61 [hep-ph/0210077] [SPIRES].

JHEP07(2009)101

[33] C.P. Buszello, I. Fleck, P. Marquard and J.J. van der Bij, *Prospective analysis of spin- and CP-sensitive variables in $H \to ZZ \to l_1^+ l_1^- l_2^+ l_2^-$ at the LHC*, *Eur. Phys. J.* **C 32** (2004) 209 [hep-ph/0212396] [SPIRES].

[34] A. Djouadi, *The Anatomy of electro-weak symmetry breaking. I: The Higgs boson in the standard model*, *Phys. Rept.* **457** (2008) 1 [hep-ph/0503172] [SPIRES].

[35] D. Rainwater, *Searching for the Higgs boson*, hep-ph/0702124 [SPIRES].

[36] K. Hagiwara and D. Zeppenfeld, *Helicity Amplitudes for Heavy Lepton Production in e^+e^- Annihilation*, *Nucl. Phys.* **B 274** (1986) 1 [SPIRES]; *Amplitudes for Multiparton Processes Involving a Current at $e^+e^-, e^\pm p$ and Hadron Colliders*, *Nucl. Phys.* **B 313** (1989) 560 [SPIRES].

[37] V.N. Gribov and L.N. Lipatov, *Deep inelastic e p scattering in perturbation theory*, *Sov. J. Nucl. Phys.* **15** (1972) 438 [SPIRES];
L.N. Lipatov, *The parton model and perturbation theory*, *Sov. J. Nucl. Phys.* **20** (1975) 94 [SPIRES];
G. Altarelli and G. Parisi, *Asymptotic Freedom in Parton Language*, *Nucl. Phys.* **B 126** (1977) 298 [SPIRES];
Y.L. Dokshitzer, *Calculation of the Structure Functions for Deep Inelastic Scattering and e^+e^- Annihilation by Perturbation Theory in Quantum Chromodynamics*, *Sov. Phys. JETP* **46** (1977) 641 [*Zh. Eksp. Teor. Fiz.* **73** (1977) 1216] SPIRES].

[38] H. Murayama, I. Watanabe and K. Hagiwara, *HELAS: HELicity Amplitude Subroutines for Feynman diagram evaluations*, KEK Report 91-11 (1992) [SPIRES].

[39] R.N. Cahn and S. Dawson, *Production of Very Massive Higgs Bosons*, *Phys. Lett.* **B 136** (1984) 196 [*Erratum ibid.* **B 138** (1984) 464] [SPIRES];
M.S. Chanowitz and M.K. Gaillard, *Multiple Production of W and Z as a Signal of New Strong Interactions*, *Phys. Lett.* **B 142** (1984) 85 [SPIRES];
S. Dawson, *The Effective W Approximation*, *Nucl. Phys.* **B 249** (1985) 42 [SPIRES];
G.L. Kane, W.W. Repko and W.B. Rolnick, *The Effective $W^\pm, Z^0$ Approximation for High-Energy Collisions*, *Phys. Lett.* **B 148** (1984) 367 [SPIRES].

[40] S. Dawson, *Radiative corrections to Higgs boson production*, *Nucl. Phys.* **B 359** (1991) 283 [SPIRES];
A. Djouadi, M. Spira and P.M. Zerwas, *Production of Higgs bosons in proton colliders: QCD corrections*, *Phys. Lett.* **B 264** (1991) 440 [SPIRES];
R.P. Kauffman and W. Schaffer, *QCD corrections to production of Higgs pseudoscalars*, *Phys. Rev.* **D 49** (1994) 551 [hep-ph/9305279] [SPIRES].

[41] M. Spira, A. Djouadi, D. Graudenz and P.M. Zerwas, *Higgs boson production at the LHC*, *Nucl. Phys.* **B 453** (1995) 17 [hep-ph/9504378] [SPIRES];
B.A. Kniehl and M. Spira, *Low-energy theorems in Higgs physics*, *Z. Phys.* **C 69** (1995) 77 [hep-ph/9505225] [SPIRES].

[42] R.P. Kauffman, S.V. Desai and D. Risal, *Production of a Higgs boson plus two jets in hadronic collisions*, *Phys. Rev.* **D 55** (1997) 4005 [*Erratum ibid.* **D 58** (1998) 119901] [hep-ph/9610541] [SPIRES].

[43] R.P. Kauffman and S.V. Desai, *Production of a Higgs pseudoscalar plus two jets in hadronic collisions*, *Phys. Rev.* **D 59** (1999) 057504 [hep-ph/9808286] [SPIRES].

JHEP07(2009)101

[44] M.A. Shifman, A.I. Vainshtein, M.B. Voloshin and V.I. Zakharov, *Low-Energy Theorems for Higgs Boson Couplings to Photons*, *Sov. J. Nucl. Phys.* **30** (1979) 711 [*Yad. Fiz.* **30** (1979) 1368] [SPIRES];
A. Djouadi, M. Spira and P.M. Zerwas, *Two photon decay widths of Higgs particles*, *Phys. Lett.* **B 311** (1993) 255 [hep-ph/9305335] [SPIRES].

[45] R.N. Cahn, M.S. Chanowitz and N. Fleishon, *Higgs Particle Production by $Z \to H\gamma$*, *Phys. Lett.* **B 82** (1979) 113 [SPIRES];
L. Bergstrom and G. Hulth, *Induced Higgs couplings to neutral bosons in e^+e^- collisions*, *Nucl. Phys.* **B 259** (1985) 137 [*Erratum ibid.* **B 276** (1986) 744] [SPIRES].

[46] K. Hagiwara, J. Kanzaki, Q. Li and K. Mawatari, *HELAS and MadGraph/MadEvent with spin-2 particles*, *Eur. Phys. J.* **C 56** (2008) 435 [arXiv:0805.2554] [SPIRES].

[47] K. Hagiwara, Q. Li and K. Mawatari, *Azimuthal angle correlation in vector-boson fusion processes at LHC*, *AIP Conf. Proc.* **1078** (2009) 235.

[48] J. Alwall et al., *MadGraph/MadEvent v4: The New Web Generation*, *JHEP* **09** (2007) 028 [arXiv:0706.2334] [SPIRES].

[49] S. Kawabata, *A New version of the multidimensional integration and event generation package BASES/SPRING*, *Comp. Phys. Commun.* **88** (1995) 309 [SPIRES].

[50] J. Pumplin et al., *New generation of parton distributions with uncertainties from global QCD analysis*, *JHEP* **07** (2002) 012 [hep-ph/0201195] [SPIRES].

[51] J.R. Andersen and J.M. Smillie, *QCD and electroweak interference in Higgs production by gauge boson fusion*, *Phys. Rev.* **D 75** (2007) 037301 [hep-ph/0611281] [SPIRES].

[52] A. Bredenstein, K. Hagiwara and B. Jager, *Mixed QCD-electroweak contributions to Higgs-plus-dijet production at the LHC*, *Phys. Rev.* **D 77** (2008) 073004 [arXiv:0801.4231] [SPIRES].

[53] K. Hagiwara, R.D. Peccei, D. Zeppenfeld and K. Hikasa, *Probing the Weak Boson Sector in $e^+e^- \to W^+W^-$*, *Nucl. Phys.* **B 282** (1987) 253 [SPIRES].

[54] R.K. Ellis, W.J. Stirling and B.R. Webber, *QCD and collider physics*, *Camb. Monogr. Part. Phys. Nucl. Phys. Cosmol.* **8** (1996) 1.

[55] D. Binosi and L. Theussl, *JaxoDraw: A graphical user interface for drawing Feynman diagrams*, *Comput. Phys. Commun.* **161** (2004) 76 [hep-ph/0309015] [SPIRES].

[56] G.F. Giudice, R. Rattazzi and J.D. Wells, *Quantum gravity and extra dimensions at high-energy colliders*, *Nucl. Phys.* **B 544** (1999) 3 [hep-ph/9811291] [SPIRES];
T. Han, J.D. Lykken and R.-J. Zhang, *On Kaluza-Klein states from large extra dimensions*, *Phys. Rev.* **D 59** (1999) 105006 [hep-ph/9811350] [SPIRES].

JHEP07(2009)101